INNOVATIONS TORONTO **2016** PRESENTS

Innovations in

Cancer Therapy & Response Monitoring

November 16 - 17, 2016

The Vaughan Estate of Sunnybrook

Toronto, Canada

Sponsors

The Terry Fox Research Institute
L'Institut de recherche Terry Fox

CIHR IRSC
Canadian Institutes of Health Research
Instituts de recherche en santé du Canada

Speakers

FEATURED

Dr. Guy Cloutier, PhD
Professor, University of Montreal

Dr. Gregory J. Czarnota, PhD, MD, FRCPC
Chief, Department of Radiation Oncology, Odette Cancer Centre
Sunnybrook Health Sciences Centre

Dr. Cheri X. Deng, PhD
Professor, Biomedical Engineering
University of Michigan

Dr. Ernest Feleppa, PhD, FIEEE, FAIUM, FAIMBE
Research Director, Lizzi Center for Biomedical Engineering,
Riverside Research

Dr. James F. Greenleaf, PhD
Professor, Mayo Clinic School of Medicine

Dr. Timothy J. Hall, PhD
Professor, Medical Physics,
University of Wisconsin School of Medicine and Public Health

Dr. Christy K. Holland, PhD
Scientific Director, Heart, Lung & Vascular Institute
Professor, Internal Medicine, Division of Cardiovascular Health and
Disease and Biomedical Engineering Program
University of Cincinnati

Dr. Robert Kerbel, PhD
Senior Scientist, Biological Sciences
Sunnybrook Research Institute

Dr. Michael C. Kolios, PhD
Professor, Department of Physics,
Ryerson University

Dr. Piotr Kozlowski, PhD
Associate Professor, Radiology/Urologic Sciences,
University of British Columbia

Dr. Oliver D. Kripfgans, PhD
Research Associate Professor, Department of Radiology
University of Michigan

Dr. William O'Brien, PhD
Professor, University of Illinois

Dr. Michael L. Oelze, PhD
Professor, University of Illinois

Dr. Tyrone Porter, PhD
Associate Professor, Boston University

Dr. Daniel Rohrbach, PhD
Researcher, Lizzi Center for Biomedical Engineering,
Riverside Research

Dr. Greg Stanisz, PhD
Senior Scientist, Physical Sciences
Sunnybrook Research Institute

Dr. Xueding Wang, PhD
Associate Professor, University of Michigan

Dr. Roger Zemp, PhD
Associate Professor, University of Alberta,
Department of Electrical & Computer Engineering

INDUSTRY

Dr. Sangeet Ghai, MD, FRCR
Lead GU Radiologist, Princess Margaret Cancer Centre,
Associate Professor, University of Toronto

Mr. Clinton Hupple, MSc
Applications Scientist, iThera Medical

Mr. Julian Lee
CEO, Alpinion Medical Systems USA

CONTRIBUTED

Dr. David Goertz, PhD
Scientist, Physical Sciences
Sunnybrook Research Institute

Dr. Emma Harris, PhD
Team Leader, Institute of Cancer Research, London,

Dr. Chris Heyn, PhD, MD, FRCPC
Radiologist, Sunnybrook Health Sciences Centre

Dr. Carl Kumaradas, PhD
Associate Professor, Department of Physics,
Ryerson University

Dr. Angus Lau, PhD
Scientist, Physical Sciences
Sunnybrook Research Institute

Dr. Pauline Muleki-Seya, PhD
Postdoctoral Fellow, Laboratoire de Mécanique et d'Acoustique,
Centre National de Recherche Scientifique
Aix-Marseille Université

Dr. Meaghan O'Reilly, PhD
Scientist, Physical Sciences
Sunnybrook Research Institute

Dr. Ali Sadeghi-Naini, PhD
Scientist, Physical Sciences
Sunnybrook Research Institute

Mr. William T. Tran
Clinical Radiation Therapist & Researcher, Odette Cancer Centre
Sunnybrook Research Institute

Posters

Authors	Title
Jay Detsky, John Conklin, Julia Keith, Sean Symons, Arjun Sahgal, Chris Heyn, Hany Soliman.	Differentiating Radionecrosis from Tumor Progression in Brain Metastases Treated with Radiosurgery: Utility of Intravoxel Incoherent Motion Perfusion MRI and Correlation with Histopathology
Golnaz Farhat, Anoja Giles, Michael C. Kolios, Gregory J. Czarnota.	Optical Coherence Tomography Spectral Analysis for Detecting Apoptosis *In Vitro* and *In Vivo*
Mehrdad J. Gangeh, Peng Chen, William T. Tran, Gregory J. Czarnota.	Deep Learning in Clinical Cancer Therapy Response Monitoring
Sayed Masoud Hashemi, Young Lee, Markus Eriksson, Håkan Nordström, James Mainprize, Arjun Sahgal, William Y. Song, Mark Ruschin.	Cone-Beam CT Image Contrast and Attenuation-Map Linearity Improvement (CALI) for Brain Stereotactic Radiosurgery Procedures
Ryan M. Jones, Meaghan A. O'Reilly, Lulu Deng, Kogee Leung, Kullervo Hynynen.	Volumetric Ultrasound-Mediated Blood-Brain Barrier Opening Using a Large Aperture Phased Array Controlled Via Passive Beamforming of Microbubble Emissions
Wilfred W. Lam, Jonathan H. Klein, Farah Hussein, Christine Tarapacki, Gregory J. Czarnota, Greg J. Stanisz.	Differentiation of Apoptosis/Necrosis from Active Tumour in Mice with Chemical Exchange Saturation Transfer (CEST) MRI
Matthew R. Lowerison, Ann F. Chambers, Hon S. Leong, Nicholas E. Power, James C. Lacefield.	Compound Speckle Model Reduces Contrast Ultrasound Variability in a Patient-Derived Xenograft Model of Renal Cell Carcinoma
Shirin Sabouri, Silvia D. Chang, Richard Savdie, Edward C. Jones, S. Larry Goldenberg, Peter C. Black, Piotr Kozlowski.	Comparing the Diagnostic Accuracy of Luminal Water Imaging with Diffusion-Weighted and Dynamic Contrast-Enhanced MRI for Evaluation of Prostate Cancer
Lakshmanan Sannachi, William Tran, Mehrdad Gangeh, Sonal Gandhi, Frances Wright, Gregory J. Czarnota.	Response Monitoring of Breast Cancer Patients Receiving Neo-Adjuvant Chemotherapy Using QUS, Texture and Molecular Features
A. J. Sojahrood, H. Haghi, R. Karshafian, M. C. Kolios.	Finite Element Simulation of the Propagation of Ultrasound Waves in a Bubbly Medium and Theoretical Considerations for Treatment Optimization
William T.Tran, Ali Sadeghi-Naini, Lee Chin, Lakshmanan Sannachi, Elyse Watkins, Sharon Lemon Wong, Belinda Curpen, Maureen Trudeau, Sonal Gandhi, Martin Yaffe, Elzbieta Slodkowska, Charmaine Childs, Gregory J. Czarnota.	Predicting Clinical and Pathological Response of Breast Tumours to Neoadjuvant Chemotherapy Using Pre-treatment Textural Features of Diffuse Optical Spectroscopic Images
Yanjie Wang, Michael C. Kolios.	Biodegradable Theranostic Agents for Breast Cancer Detection and Therapy Using Photoacoustic Technique
Lauren A. Wirtzfeld, Eric M. Strohm, Michael C. Kolios.	Ultrasound and Photoacoustic Analysis of HT-29 and AML Cell Pellets at 200 MHz
Jason Vickress, Michael Lock, Aaron Leung, Stewart Gaede, Rob Barnett, Slav Yartsev.	Potential Benefit of Rotational Radiation Delivery

Itinerary

Innovations in Cancer Therapy & Response Monitoring
Wednesday, November 16th, 2016

Presenter	Time	Title
BREAKFAST	**08:00 – 08:45**	
G. Czarnota & M. Kolios	08:45	Welcome & Introduction
R. Kerbel	09:00	Implications of 'Vessel Co-option' by Tumors for Antiangiogenic Therapy of Metastatic Disease
TISSUE CHARACTERIZATION & ELASTOGRAPHY I - Chaired by M. Kolios		
G. Czarnota	09:30	*A Priori* Prediction of Neoadjuvant Chemotherapy Response and Survival in Breast Cancer Patients Using Quantitative Ultrasound
W. O'Brien	09:50	Quantitative Ultrasound: Some Interesting Outcomes
M. Oelze	10:10	The Potential of Monitoring of Focused Ultrasound Treatment of Tumors using Quantitative Ultrasound
BREAK	**10:30 - 11:00**	
SHEARWAVE & PHOTOACOUSTICS I - Chaired by G.Stanisz		
M. Kolios	11:00	On the Potential of Photoacoustic Tissue Characterization for Cancer Treatment Monitoring
R. Zemp	11:20	Multimodal Photoacoustic- Ultrasound Molecular Imaging and Biomarker Diagnostics
X. Wang	11:40	Evaluating Histological Microfeatures and Microenvironment of Cancer *in Vivo* by Photoacoustic Techniques
E. Harris	12:00	Shear-Wave Elastography
LUNCH	**12:15 – 14:05**	
THERAPY & THERAPY MONITORING I - Chaired by G. Czarnota		
C. Holland	14:05	Ultrasound-Mediated Drug Delivery for Cardiovascular Disease
C. Deng	14:25	Acoustic Tweezing Cytometry for Mechanobiology Investigations
O. Kripfgans	14:45	Microbubbles for Cavitation Enhanced Treatment- Non-Invasive Tissue Reduction for Treatment of Hypertrophic Cardiomyopathy
C. Kumaradas	15:05	Picosecond Cell Nanosurgery using Gold Nanoparticle Assemblies
BREAK	**15:20 - 15:50**	
J. Lee	15:50	Alpinion Clinical Research Ultrasound System
M. O'Reilly	16:05	Ultrasound-Mediated Drug Delivery for the Treatment of Leptomeningeal Metastases
D. Goertz	16:20	Potentiating Anticancer Agent Effects with Ultrasound Stimulated Microbubbles
POSTER SESSION & HORS D'OEUVRES	**16:45 - 18:30**	
DINNER	**18:30-20:30**	

Innovations in Cancer Therapy & Response Monitoring

Thursday, November 17th, 2016

Presenter	Time	Title
BREAKFAST	**08:00 – 09:00**	
SHEARWAVE/PHOTOACOUSTICS II - Chaired by G. Stanisz		
G. Cloutier	09:00	Improvement of Solid Breast Lesion Classification by Adding Homodyned K Modeling to Shear Wave Elastography
J. Greenleaf	09:20	Shear Wave Speed Differentiates Lymph Nodes in Breast Cancer Patients
C. Hupple	09:40	Detecting Tumour Response to a Vascular Disrupting Agent using Multispectral Optoacoustic Tomography
A. Sadeghi-Naini	09:55	Imaging-Based Analysis of Intratumour Heterogeneity for Monitoring Response to Anticancer Therapies
BREAK	**10:10 - 10:40**	
TISSUE CHARACTERIZATION & ELASTOGRAPHY II - Chaired by M. Oelze		
S. Ghai	10:40	Clinical Applications of 29 MHz Micro-Ultrasound for Targeted Prostate Biopsies
D. Rohrbach	10:55	Prostate Cancer Imaging at High Frequencies using Quantitative Micro-Ultrasound
E. Feleppa	11:15	3D QUS for Better Detection of Lymph Node Metastases and Improved Staging and Treatment of Cancer
T. Hall	11:35	Improving Specificity in Breast Imaging
P. Muleki-Seya	11:55	Nonlinear Ultrasound Parameters to Monitor Mitotic Catastrophe or Apoptosis in Cell Pellet Biophantoms
LUNCH	**12:10 - 13:45**	
THERAPY & THERAPY MONITORING II - Chaired by M. Kolios		
T. Porter	13:45	Cavitation-Enhanced Ultrasound-Mediated Tumor Ablation Nucleated with Phase-Shift Nanoemulsions
G. Czarnota	14:05	Ultrasound-Stimulated Microbubble Enhancement of Radiation Responses
G. Stanisz	14:25	MRI of Cancer Therapies
P. Kozlowski	14:45	Luminal Water Imaging- A Novel Quantitative MRI Technique for Prostate Cancer Diagnosis
BREAK	**15:05 - 15:20**	
A. Lau	15:20	Opportunities for Rapid MRI in Radiation Oncology
C. Heyn	15:35	Evolution of Perfusion Parameters in Brain Metastases Treated with Stereotactic Radiosurgery in the First Month after Treatment: Comparison of Dynamic Contrast Enhanced MRI and Intravoxel Incoherence Motion
W. Tran	15:50	Predicting Clinical and Pathological Response of Breast Tumours to Neoadjuvant Chemotherapy Using Pre-treatment Textural Features of Diffuse Optical Spectroscopic Images
CLOSING REMARKS	**16:05-16:15**	

Speaker Abstracts

Improvement of Solid Breast Lesion Classification by Adding Homodyned K Modeling to Shear Wave Elastography

Guy Cloutier (1,2), François Destrempes (1), Julian Garcia Duitama (1), Louise Allard (1), Boris Chayer (1), Lucie Lalonde (3), Maude Labelle (3), Mona El Khoury (3), Isabelle Trop (3)

(1) Laboratory of Biorheology and Medical Ultrasonics, University of Montreal Hospital Research Center, Montréal, QC, Canada, H2X 0A9

(2) University of Montreal, Department of Radiology, Radio-Oncology and Nuclear Medicine, and the Institute of Biomedical Engineering, Montréal, QC, Canada, H3T 1J4

(3) Department of Radiology, Beast Imaging Center, University of Montreal Hospital, Montréal, QC, Canada, H2W 1T8

Email: guy.cloutier@umontreal.ca

ABSTRACT

Introduction: The goal was to provide an ancillary tool to the Breast Imaging Reporting and Data System (BI-RADS) classification of solid breast lesions at ultrasonography (US) prior to biopsy.

Materials and Methods: This study received institutional review board approval, and all subjects provided informed consent. Sixty women (mean age, 52 years; age range, 15–92 years) with indeterminate solid breast lesions (BI-RADS categories 4–5; mean size: 15.6 mm; range: 4.4–42.9 mm) were enrolled. Prior to biopsy, additional radiofrequency US images were obtained, and a 3-second cine sequence was used. In addition, shear-wave (SW) elastography measurements were acquired with the same echograph. The research data were analyzed at a later time and were not used to modify patient management decisions. The lesions were segmented manually in a reference frame of each cine loop of US images and in the elastography images. An automatic algorithm then propagated the lesion contours on all images of each loop. The radiofrequency US images were compensated for tissue attenuation based on a spectral fit method. Three regions-of-interest were considered for analysis: the intratumoral zone, a 3-mm supratumoral zone, and a 5-mm infratumoral zone. Three parameters of the homodyned *K* distribution (α, μ_n and k values) were extracted in each of the three regions: the scatterer clustering parameter α, the mean intensity normalized by the maximal intensity μ_n, and the coherent-to-diffuse signal ratio k. In addition, the maximal elasticity value in the intratumoral zone was considered, for a total of 10 features. The mean decrease in accuracy was used as a measure of variable importance for feature selection. The selected features in decreasing order of importance were: the intratumoral elastography measurement, the supratumoral k, the intratumoral k, and the supratumoral α. The random forests package of the statistical software R was used for classification of the sixty lesions as benign versus malignant. To assess the proposed classification scheme, the 0.632+ bootstrap technique was applied, with 1000 bootstraps, using stratified sampling with repetition. To produce the receiver operating characteristic (ROC) curve, stratified sampling was performed with a variable weight.

Results and Discussion: Among the sixty lesions, 21 were classified as BI-RADS category 4A lesions, 9 as BI-RADS category 4B lesions, 4 as BI-RADS category 4C lesions, and 26 as BI-RADS category 5 lesions. There were 28/60 malignant lesions (46.7%). The area under the ROC curve (AUC) increased by a factor of 11% when using the selected features in comparison with the elastography measurement only. The benefit of considering quantitative US cellular imaging features in addition to elasticity seems potentially useful to improve the patient diagnostic.

Keywords: Ultrasound, Breast cancer, Homodyned K-distribution, Elastography, Statistical Learning.

Ultrasound-Stimulated Microbubble Enhancement of Radiation Responses

Ahmed El Kaffas (1,2), Anoja Giles (1,2), Gregory J. Czarnota (1,2)

(1) Sunnybrook Health Sciences Centre, Toronto, Canada
(2) University of Toronto, Toronto, Canada

Email: Gregory.Czarnota@sunnybrook.ca

ABSTRACT

Introduction: We have recently demonstrated that ultrasound-stimulated microbubble treatment may be used to enhance radiation responses. Recent analyses in vitro and in vivo have demonstrated that this is related to the production of Asmase-induced ceramide in response to radiation-induced cell membrane damage. Here we further investigate the importance of the Asmase pathway.

Materials and Methods: Experiments were carried out in wild-type (C57BL/6) or *asmase*-knockout animals, implanted with fibrosarcoma xenografts (MCA-129). A cohort of wild-type animals received the endothelial ASMase-ceramide pathway inhibitor sphingosince-1-phosphate (S1P). Animals were treated with radiation doses of 0-8 Gy with or without *a priori* USMB exposure at varying microbubble concentrations. Treatment response was assessed with high-frequency 3D Doppler ultrasound acquired at baseline, and at 3, 24 and 72 hours after treatment and the vascular index (VI) was used to quantify imaging. Immunohistochemistry (ISEL, ceramide and CD31) of
tumour sections served to complement imaging and further assess treatment response.

Results and Discussion: Results confirmed a dose-dependent synergistic decrease in VI of greater than 40% by 3 hours following radiation and USMB. This peaked at 24 hours following treatment, persisting for up to 72 hours, and was accompanied by extensive tumour cell death. In contrast, minimal decreases in tumour perfusion (power Doppler/CD31) or cell death (ISEL) were noted in S1P-treated and *asmase* knockout animals for all treatments. Results are the first to demonstrate the importance of the ASMase-ceramide pathway in mechanotransductive vascular targeting using USMB radiation enhancement. These further confirm that an acute vascular effect is necessary for rapid tumour cell death, and that a vascular effect can be elicited at low radiation doses (< 8 Gy) by *a priori* USMB exposure.

Keywords: ASMase, Sphingomyelinase, radiation therapy, endothelial cells, ceramide, radiosensitization, microbubbles, mechanotransduction

A Priori Prediction of Neoadjuvant Chemotherapy Response and Survival in Breast Cancer Patients using Quantitative Ultrasound

Hadi Tadayyon (1,2), William Tran (1,2), Farnoosh Hadizad (1,2), Gregory J. Czarnota (1,2)

(1) Sunnybrook Health Sciences Centre, Toronto, Canada
(2) University of Toronto, Toronto, Canada

Email: Gregory.Czarnota@sunnybrook.ca

ABSTRACT

Introduction: Quantitative ultrasound (QUS) can probe tissue structure and analyze tumour characteristics. We have used it previously to monitor the early effects of chemotherapy with results indicating imaging-outcomes obtained one week after therapy initiation can predict ultimate clinical outcomes of patients.

Materials and Methods: Using a 6-MHz ultrasound system, radiofrequency data were acquired from 56 locally advanced breast cancer patients prior to their NAC and QUS texture features were computed from regions of interest in tumour cores and their margins as potential predictive and prognostic indicators. Breast tumor molecular features were also collected and used for analysis.

Results and Discussion: A multiparametric QUS model was constructed, which demonstrated a response prediction accuracy of 88% and ability to predict patient 5-year survival rates ($p=0.01$). QUS features demonstrated superior performance in comparison to molecular markers and the combination of QUS and molecular markers did not improve response prediction. This study demonstrates for the first time, that non-invasive QUS features in the core and margin of breast tumours can indicate breast cancer response to neoadjuvant chemotherapy (NAC) and predict five-year recurrence-free survival.

Keywords: Quantitative Ultrasound, Ultrasound Spectroscopy, Tumour Response Assessment, Prognostic Biomarker

Acoustic Tweezing Cytometry for Mechanobiology Investigations

Cheri X. Deng (1), Jianping Fu (1,2)

(1) Department of Biomedical Engineering, University of Michigan, Ann Arbor, Michigan 48105, USA
(2) Departments of Mechanical Engineering, University of Michigan, Ann Arbor, Michigan 48105, USA

Email: cxdeng@umich.edu

ABSTRACT

Introduction: Mechanosensitivity of mammalian cells to extracellular mechanical signals are central to many important developmental, physiological, and pathological processes, affecting critical cell functions including growth, migration, differentiation, and apoptosis[1]. Mechanical stimulation is critical in controlling many important functions of mammalian cells, including cell spreading, contractility, gene expression, and even stem cell differentiation. However, the exact molecular mechanisms underlying mechanotransduction, despite much recent progress, are still elusive, limited by the availability of tools that are capable of applying controlled mechanical forces to cells to elicit and assess cellular responses. Therefore, we develop acoustic tweezing cytometry (ATC) utilizing ultrasound-excitable microbubbles targeted to cells to generate controlled subcellular mechanical forces to live single cells.

Materials and Methods: Early passages (2 – 4) of NIH 3T3 mouse fibroblasts, human mesenchymal stem cells (hMSCs) as well as hESC line H1 were used in this study. Targesphere™-SA microbubbles (Targeson) (mean diameter 1.8 ± 0.2 μm, n = 208) and biotinylated Arg-Gly-Asp (RGD) peptides were used to form RGD-coated microbubbles to conjugate to cells. Acetylated low density lipoprotein (AcLDL)-coated microbubbles were also formed and conjugated with cells for separate experiments. A 1.25 MHz planar circular transducer or a 10 MHz focused transducer were used to generate ultrasound pulses with desired parameters including acoustic pressure, pulse duration, pulse repetition frequency (PRF). The *in situ* bubble activities during ATC were recorded by high-speed imaging system. A customized algorithm in Matlab was developed to track the size and translational displacement of the bubbles to investigate its potential correlation with the cell cytoskeleton (CSK) contractile force response. As cellular contractile forces are critical in regulating cellular functions, we quantified the contractile forces of the cells exposed to ATC utilizing an elastomeric micropost array as subcellular live-cell force sensors.

Results and Discussion: By applying ultrasound pulses to excite lipid microbubbles attached to cell integrin receptors, we show that we can apply subcellular mechanical forces to mechanosensitive cells such as NIH/3T3 fibroblasts. ATC application elicited a rapid and sustained reactive intracellular cytoskeleton contractile force increase in different adherent mechanosensitive cells. Further, ultrasound-mediated intracellular cytoskeleton contractility enhancement was dose-dependent and required an intact actin cytoskeleton as well as RhoA/ROCK signaling. We also show that by acoustically actuating integrin-bound microbubbles (MBs) targeted to hESCs, ATC increased the survival rate and cloning efficiency of hESCs by 3-fold. A positive correlation was observed between the increased hESC survival rate and total accumulative displacement of integrin-anchored MBs during ATC stimulation.

Compared to magnetic and optical tweezers, ATC technique has several unique advantages. Microbubbles have been established as an effective ultrasound imaging contrast agent, and as a potential drug carrier. Thus, ATC has the potential for imaging guided manipulation of cellular contractility and downstream effects. Besides direct mechanical perturbation of cells, sonoporation may also be seamlessly integrated in the same platform with ATC to deliver membrane-impermeable drugs into cells for additional biochemical modulations of intracellular signaling.

Cells can sense mechanical stimuli and convert them into downstream intracellular biochemical signals, and such mechanotransduction process has profound impact in many physiological and pathological contexts. For example, cytoskeleton contractility has been implicated as a non-destructive live-cell predictor for hMSC differentiation. Thus, our ATC can be effectively applied, in principle, to regulate biomechanical and cellular responses of different cell types. The strong contractile response of NIH/3T3 fibroblasts as well as hMSCs to ATC suggests that our technique may have a great utility in regulating cellular behaviors. With the ability to enhance hESC survival, ATC may serve as a promising biocompatible tool to improve hESC culture.

Keywords: Ultrasound, Microbubbles, Integrin, Contractile Forces, Mechanobiology, Embryonic Stem Cells, Mesenchymal Stem Cells

3D QUS for Better Detection of Lymph-Node Metastases and Improved Staging and Treatment of Cancer

Ernest J. Feleppa (1), Jonathan Mamou (1), Junji Machi (2), Maoxin Wu (3), Ying Fan (4), Emi Saegusa-Beecroft (2), Alain Coron (5)

(1) Lizzi Center for Biomedical Engineering, Riverside Research, New York, NY, USA, 10038
(2) University of Hawaii and Kuakini Medical Center, Honolulu, HI, USA, 96817
(3) State University of New York and Stony Brook Medicine, Stony Brook, NY, USA, 11794
(4) GE Global Research, Niskayuna, NY, USA, 12309
(5) Sorbonne Universités, UPMC Univ Paris 06, CNRS, INSERM, Laboratoire d'Imagerie Biomédicale (LIB), 75006, Paris, France

Email: EFeleppa@RiversideResearch.org

ABSTRACT

Introduction: Decisions regarding cancer treatment are based on TNM staging: evaluations of primary-tumor features (T), the degree of lymph-node involvement (N), and the extent of metastases to distant sites (M). Our quantitative-ultrasound (QUS) studies are directed toward the second evaluation: assessment of lymph-node involvement. If metastases are not present in lymph nodes, then the cancer is considered to be localized and local treatment can be applied with minimal side effects and cost. If metastases are detected in lymph nodes, then the cancer is considered to be systemic and is treated with therapies that may have severe side effects and high costs. Our QUS methods are intended to improve detection of small, but clinically significant metastases that easily can be missed by current histology methods. These methods typically examine only central sections of dissected lymph nodes; they can overlook small metastases that are not in the center of the lymph node and can lead to understaging and therefore to inappropriate treatment.

Materials and Methods: Lymph nodes were surgically excised from colorectal-, gastric-, and breast-cancer patients for staging purposes; dissected from the excised surgical specimen; and scanned in a saline bath using a 26-MHz transducer. Echo signals were digitized at 25-μm steps in X and Y directions over the full volume of the lymph node. After segmentation to select lymph-node tissue for analysis and to correct for attenuation within the surrounding fat as well as nodal tissue, QUS-parameter estimates were calculated in 3D from the RF echo signals using overlapping cylindrical regions of interest that were 1 mm in diameter and length. 3D renderings of B-mode images and parameter images of QUS-estimate values were generated. Scanned lymph nodes were inked to recover orientation, then fixed, embedded, and serially thin sectioned in steps of 50 or 100 μm, depending on the size of the lymph node. Cancer foci were demarcated in every thin section that contained them. Using the ink colors as a reference, the sections were reconstructed into a 3D histology volume co-registered with the 3D reconstruction of the ultrasound-based volumes. Using linear-discriminant methods with the histology as a gold standard, lymph-node tissue was classified as cancerous or non-cancerous based on QUS-parameter values. Leave-one-out, cross validation was used with ROC methods to assess and express classification performance.

Results and Discussion: Areas under the ROC curve exceeded 0.96 for colorectal- and gastric-cancer cases and 0.86 for breast-cancer cases. Images of cancer likelihood in 3D, QUS-based images showed strong correlation with cancer foci in 3D, histology images. High-frequency QUS methods potentially can provide a reliable means of directing pathologists to otherwise missed micrometastases. Extension of these methods to lower frequencies can help pathologists identify cancerous lymph nodes in surgical specimens and can enable surgeons to select nodes preoperatively or intraoperatively for excision.

Keywords: TNM Staging; Cancer Staging; Lymph Nodes; Metastases; Treatment Planning

Clinical Applications of 29 MHz Micro-Ultrasound for Targeted Prostate Biopsies

Brian Wodlinger (1), Sangeet Ghai (2)

(1) Exact Imaging, 7676 Woodbine Ave., Markham, ON Canada L3R 2N2
(2) Princess Margaret Cancer Center, University Health Network, 610 University Ave, Toronto, ON Canada M5G 2M9

Email: Sangeet.Ghai@uhn.ca

ABSTRACT

Introduction: The current standard of care for prostate cancer detection is transrectal ultrasound (TRUS) guided biopsies using conventional (7 – 12 MHz) ultrasound. This imaging modality is limited in its detection of significant cancer and has high (30 – 40%) false negative rates. A novel micro-ultrasound system operating at 29 MHz has been introduced that has the potential to visualize suspicious regions in the prostate and allow urologists to target their biopsies at those suspicious regions, thereby potentially improving the real-time targeting of biopsies, and consequently improving the standard of care.

Materials and Methods: A novel high resolution 29 MHz micro-ultrasound system (ExactVu™ micro-ultrasound, Exact Imaging, Markham, Canada) is currently being used in an ongoing 2,000 patient adaptive, multi-site clinical trial to explore the improved detection rate of micro-ultrasound TRUS vs. conventional TRUS as well as the improved sensitivity and specificity of targeting with micro-ultrasound TRUS vs. conventional TRUS. In addition, a novel risk identification protocol - - PRI-MUS™ (prostate risk identification using micro-ultrasound) has been developed to aid in targeting suspicious regions. The ongoing clinical trial will also prospectively evaluate the ability of this novel protocol to aid in detecting significant cancer in the micro-ultrasound images.

Results and Discussion: While the trial is ongoing and results are not yet available, significant benefits are evident. First, the 70 – 100-micron resolution at 29 MHz allows urologists to view anatomical targets and tissue characteristics not seen with conventional ultrasound. Second, the PRI-MUS protocol, which has been recently published*, shows that with only 1 hour of training all investigators achieved statistical significance using PRI-MUS to detect cancer in micro-ultrasound cine loops (verified by pathology). Third, the current system also has significant potential to provide a base on which to build an evidence-based *multi-parametric ultrasound protocol* including functional imaging such as micro-Doppler, contrast mode, and other multi-parametric capabilities which are planned for the platform. In summary, there is significant clinical potential for leveraging the new visualization and targeting capabilities of high resolution micro-ultrasound in biopsy guidance and detection of prostate cancer.

*Ghai, S. et al, "**Assessing *Cancer Risk in Novel 29 MHz Micro-Ultrasound Images of the Prostate: Creation of the PRI-MUS (prostate risk identification using micro-ultrasound) protocol***", *Journal of Urology, 2016 Aug;196(2):562-9.*

Keywords: micro-ultrasound, targeted prostate biopsies, high resolution ultrasound, TRUS

Potentiating Anticancer Agent Effects with Ultrasound Stimulated Microbubbles

Sharshi Bulner (1,2), Aaron Prodeus (1), Niroo Sivapalan (1), Margarita Todorova (1,2), Robert Kerbel (1,2), Jean Gariepy (1,2), Kullervo Hynynen (1,2), David Goertz (1,2)

(1) Physical Sciences, Sunnybrook Health Sciences Centre, Toronto, ON, Canada
(2) Department of Medical Biophysics, University of Toronto, Toronto, ON, Canada

Email: goertz@sri.utoronto.ca

ABSTRACT

Introduction: Considerable efforts are being directed towards investigating the use of ultrasound stimulated microbubbles (USMBs) to promote the uptake of anticancer agents in tumors. It has also been shown that USMBs can induce a rapid shutdown of the tumor vasculature. This effect can be accompanied by tumor growth inhibition but eventually there is a degree of flow recovery along with the resumption of tumor growth. These effects parallel those observed for small molecule vascular disrupting agents, which have shown the most effective antitumor effects when combined with other anticancer agents. In this presentation we will describe work that has been conducted combining the antivascular USMB effects with anti-angiogenic approaches and an immunotherapeutic agent.

Materials and Methods: All work was carried out on tumors that were subcutaneously implanted in mice. 1 MHz ultrasound was employed using a series of 50ms bursts transmitted at 20s intervals to permit reperfusion between exposure sequences. Exposures were conducted for a period of 2 minutes following the systemic injection of microbubbles. Pressure levels ranged from 1.4-1.65 MPa which was observed to produce high levels of inertial cavitation. Flow within the tumors was monitored during treatments with ultrasound contrast imaging. For each treatment type, both longitudinal growth experiments were conducted along with acute experiments to acquire tissue for histologic analyses (apoptosis, necrosis, proliferation and perfusion). Experiments were carried out combining USMB treatments with metronomically administered cyclophosphamid (MCTX) for MDA-231-MB tumors, and Sorafenib for hepatocellular carcinoma tumors (Hep3b). An immunotherapy approach was investigated by combining the USMB treatments with anti-PD-1 for the colorectal tumor model CT26.

Results and Discussion: For all tumor models, the USMB treatments at produced a rapid and pronounced vascular shutdown within the tumors and resulted in a significant but modest growth inhibition relative to the control (sham) groups. For the longitudinal therapy experiments, the combined USMB+drug groups had profound and significant growth inhibition relative to both the USMB-only and drug-only groups. A histologic analysis of the tumors from the acute experiments (24 hour point) revealed a higher level of apoptosis and necrosis and lower levels of proliferation in the combined versus individual treatment groups. For MCTX and Sorafenib, both of which exert potent antiangiogenic effects, the perfusion staining results indicated that a vascular ‘rebound’ effect for the USMB treatments was blunted, suggesting that this was one mechanism of synergy. For the anti-PD-1 study, flow cytometry results indicated an impact of the treatments on tumor infiltrating lymphocytes. Collectively, these results suggest the considerable potential of this approach to potentiate the effects of anticancer agents. A range of application areas are possible, such as the treatment of primary and metastatic tumors situated in the liver.

Keywords: Ultrasound Stimulated Microbubbles (USMBs)

Shear Wave Speed Differentiates Lymph Nodes in Breast Cancer Patients

James Greenleaf (1), Matthew Urban (1), Shigao Chen(1), Azra Alizad (1)

(1) Department of Physiology and Biomedical Engineering, Mayo Clinic College of Medicine, Rochester MN USA

Email: jfg@mayo.edu

ABSTRACT

Introduction: Shear wave ultrasound elastography uses a push beam to move hour glass shaped region of tissue that induces a shear wave propagating away from the push. The speed of the shear wave is related to the stiffness of the tissue. The shape of the shear wave is complex and decreases in amplitude quickly with distance traveled. Using multiple pushes in the region of interest can provide more shear motion over a larger area. We have developed a method of measuring and untangling these shear waves to obtain a measure of shear wave speed in a larger region of interest. These techniques have been implemented on a commercial ultrasound machine that we used to measure speed within lymph nodes of breast cancer patients.

Materials and Methods: We studied 26 female patients with breast cancer. Shear wave speed was measured in lymph nodes suspected to be positive due to B-mode ultrasound. The lymph nodes were then biopsied. With a stiffness cutoff of 27.6 kPa we obtained a sensitivity of 100% and specificity of 86% for positive vs negative biopsies in the lymph nodes.

Results and Discussion: These results, when combined with others in the literature and extended with many more patients, may lead to a useful approach to staging breast cancer using ultrasound deduced lymph node stiffness among other indicators.

Keywords: Breast Cancer, Shear Wave, Elastography, Lymph Nodes, Specificity, Sensitivity.

Improving Specificity in Breast Imaging

Timothy J Hall (1), Haidy G Nasief (1), Ivan M Rosado-Mendez (1), James A Zagzebski (1), Assad A Oberai (2), Paul E Barbone (3)

(1) Medical Physics Department, University of Wisconsin, Madison, WI USA 53705
(2) Scientific Research Computation Center (SCOREC), Rensselaer Polytechnic Institute, Troy, NY USA 12180
(3) Department of Mechanical Engineering, Boston University, Boston, MA USA 02215

Email: tjhall@wisc.edu

ABSTRACT

Introduction: We use quantitative ultrasound (QUS) techniques, including parameters based on the echo signal power spectrum and measures of tissue elasticity, to objectively describe the underlying tissue microstructure with the hope of improving breast ultrasound specificity. Individually, and in combination, many of these parameters have demonstrated promise in differentiating benign from malignant masses. However, the estimated values for some parameters, such as those based on measures of echo signal coherence, suggest that in certain cases, assumptions used to estimate power spectra over a region are violated. We have developed a systematic approach to characterize echo signal statistics and, within the formalism of the Reference Phantom Method, obtained system-independent measures of tissue properties when they contribute significantly to backscatter (e.g., resolvable and sub-resolution scatterers that have periodic spacing, strong isolated scatterers and specular reflectors, scatterers with a low number density). Testing assumptions and validating the analysis approach should increase confidence in results and reduce bias and variance in the parameter estimates. Current studies independently assess and interpret QUS parameters and elasticity parameters, but they both are closely related to the same underlying tissue microstructure. It seems likely that much can be learned by coupling these studies more closely.

Materials and Methods: Patients referred for ultrasound-guided core biopsy of a suspicious mass were recruited into an IRB-approved and HIPAA-compliant protocol for elasticity imaging and QUS assessment. Clinical ultrasound imaging systems from Siemens (Elegra, Antares, and S2000) were used to scan the breast in the supine position. A phantom with known properties (produced and calibrated in our lab using standard techniques) was scanned to allow the use of the Reference Phantom Method for QUS analysis. A systematic approach was used to estimate the contribution from scattering sources that provide coherence in the echo signals. Among data from nearly 500 subjects, we selected the subset that met criteria for quality and completeness (associated reference phantom scans; pathology report) and further partitioned the benign class to include only fibroadenomas, significantly simplifying the task. This resulted in a data set of 27 fibroadenomas and 16 cancers. QUS parameter estimates were assessed independently and in combinations of parameters using a minimum Mahalanobis distance Bayesian classifier. Area under the ROC curve was used to judge performance.

Results and Discussion: No single QUS parameter provides perfect differentiation between benign and malignant disease. However, the Bayesian classifier successfully differentiated all fibroadenomas from all cancers using 3 parameters (attenuation, effective scatterer diameter, ESD heterogeneity) in a biased pool of high-quality data. Separately, elasticity parameters also perform well (80% specificity at 100% sensitivity) in a smaller pool of data. It is interesting that two parameters that appear powerful in differentiating benign from malignant masses are measures of parameter heterogeneity within the tumor. The coupling of elasticity imaging and backscatter QUS studies will be discussed. The need to increase the size of the data set is clear – a larger pool of data will allow inclusion of more QUS parameters in a statistical model. Extensions to 3D, currently underway, will likely improve screening with ultrasound.

Keywords: Coherence, Elasticity, Heterogeneity, Bayesian Classifier

A Cross-Machine and Cross-Breast Comparison of Shear-Wave Speed Measurements in the Normal Female Breast

Srikanta Sharma (1), Ruchi Sinnantamby (2), Elizabeth O'Flynn (1), Anna M. Kirby (1), Jeffery C. Bamber (1)
Emma J. Harris (1)

(1) The Institute of Cancer Research and Royal Marsden NHS Foundation Trust, London, UK, SM2 5PT
(2) Cambridge University Hospitals NHS Foundation Trust, Cambridge, UK, CB2 0QQ

Email: eharris@icr.ac.uk

ABSTRACT

Introduction: We propose to test shear-wave speed (SWS) as a useful quantitative biomarker of radiation-induced breast toxicity by measuring differences in SWS between the ipsilateral and contralateral breasts of women with clinically diagnosed breast hardness post breast radiotherapy at two UK RT centers. This approach assumes that SWS is similar in both breasts prior to therapy. Measures of SWS must also be reproducible across the two centers, which use different ultrasound machines. This study tests for differences in absolute values of SWS measured between breasts using two different ultrasound scanners at different UK centers on healthy volunteers.

Materials and Methods: Four healthy volunteers were recruited for this study. The Aixplorer® (Supersonic Imagine) and S2000® (Siemens) machines were used. Cross-center, (cross-operator and cross-machine) measurements were performed on an ultrasound elasticity phantom (Model 049A, CIRS) and volunteers at both centers on the same day. Eight images were acquired from each breast with the transducer in radial and anti-radial orientations (see Fig.1) and without pre-compression. Wilcoxon and Man Whitney-U tests were used to test for differences in median SWS between the centers, breasts and transducer orientations in skin, subcutaneous fat and glandular tissues.

Results and Discussion: There were no significant differences in SWS measurements in the phantom between machines. There were, however, significant difference in the SWS estimates *in vivo* between machines for all breast tissues. The mean SWS values from skin, fat and glandular tissues measured with Aixplorer and S2000 were: 2.71 & 1.66 ms^{-1}, 2.83 & 1.29 $ms^{-1}$and 1.89 & 1.33 ms^{-1}respectively (p-values <<0.01)(Fig.2). The SWS values were significantly different between skin and glandular tissue for both machines. Image artifacts were clearly visible in Aixplorer images and may account for cross-machine differences in vivo. There were significant differences between the SWS of the skin between breasts (p-values <<0.01). Variation in absolute measurements of SWS *in vivo* may restrict the use of SWS as a useful quantitative biomarker of breast tissue stiffness. For an individual machine, there was little variation between breasts, indicating that the contralateral breast may be used a control for measures of radiation-induced toxicity.

Keywords: Shear-wave elastography; Radiation toxicity; Breast radiotherapy

Fig. 1. Illustration of transducer positions used to acquire SWS measurements from the breast.

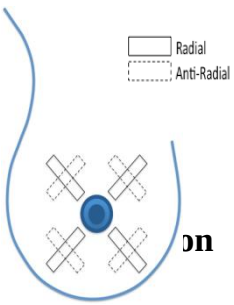

Fig. 2. Box and whisker plots of shear-wave speed measurements for Aixplorer and S2000 in different breast tissues. (*** p-value << 0.001)

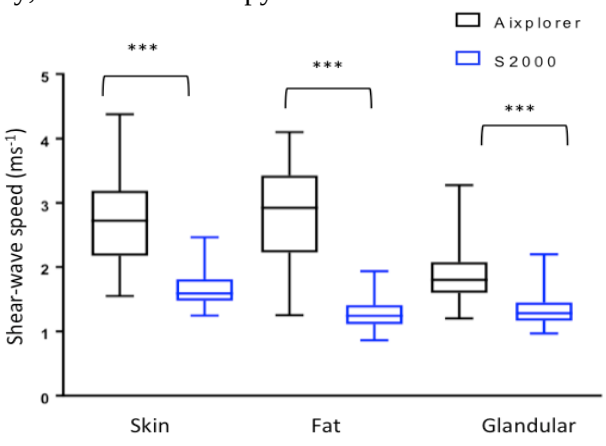

Metastases Treated with Stereotactic Radiosurgery in the First Month After Treatment: Comparison of Dynamic Contrast Enhanced MRI and Intravoxel Incoherent Motion

Anish Kapadia (1), Hatef Mehrabian (2), John Conklin (1,3), Sean Symons (1), Pejman Maralani (1), Greg Stanisz (2) Arjun Sahgal (3), Hany Soliman (3), Chris Heyn (1)

(1) Department of Medical Imaging, Sunnybrook Health Sciences Centre, Toronto, ON Canada M4N 3M5
(2) Department of Physical Sciences, Sunnybrook Research Institute, Toronto, ON Canada M4N 3M5
(3) Department of Radiation Oncology, Sunnybrook Health Sciences Centre, Toronto, ON, Canada, M4N 3M5

Email: chris.heyn@utoronto.ca

ABSTRACT

Introduction: Stereotactic radiosurgery (SRS) of brain metastases results in injury to tumour endothelium and profound reduction in blood flow occurring hours to days after treatment. This reduction in blood flow and ensuing tumour ischemia is hypothesized to play an important role in the therapeutic response of metastases to SRS. While this radiobiology has been extensively studied in animal models, there is little human data examining changes in tumour blood flow early after SRS. The purpose of this study was to characterize changes in tumour blood flow using two different MRI techniques: dynamic contrast enhanced (DCE)-MRI and intravoxel incoherent motion (IVIM) in the first week and month after SRS of brain metastases.

Materials and Methods: Seventeen patients with a total of 21 brain metastases were scanned prior to treatment, and at 1 week and 1 month after SRS. Tumour blood volume was measured using DCE-MRI and IVIM which provide measurements of plasma volume fraction (v_p) and perfusion fraction (f) respectively. Changes in DCE-MRI and IVIM parameters were evaluated by paired t-test or Wilcoxon signed-rank test. Linear regression between blood volume measured using DCE-MRI and IVIM was performed and the Pearson correlation coefficient was calculated.

Results and Discussion: No significant change in blood volume measured using DCE-MRI or IVIM was observed at 1 week. DCE-MRI measurement of blood volume (v_p) showed a statistically significant decrease at 1 month. IVIM measurement of blood volume (f) showed an opposite trend with a statistically significant increase at 1 month. DCE-MRI and IVIM measurements of blood volume appeared poorly correlated at baseline (r=0.33) and this correlation worsened after treatment (r=0.14 and 0.3 at 1 week and 1 month respectively).

In summary, MRI measurements of tumour perfusion fail to show significant change at 1 week post SRS. Significant changes in blood volume were found at 1 month for both MRI techniques with DCE-MRI agreeing with expected radiobiology and IVIM showing contradictory behaviour. These results support the use of DCE-MRI for studying changes in tumour perfusion after SRS and raise questions about the validity of the IVIM methodology.

Keywords: Brain Metastases; Magnetic Resonance Imaging; Perfusion

Ultrasound-Mediated Drug Delivery for Cardiovascular Disease

Christy K. Holland (1), J. T. Sutton (1,2), K. J. Haworth (1), S. K. Shanmukhappa (3)

(1) College of Medicine, Internal Medicine, Division of Cardiovascular Health and Disease, and Biomedical Engineering Program, University of Cincinnati, ML 0586, 231Albert Sabin Way, Cincinnati, OH, 45208
(2) Philips Research North America, Cambridge, MA, USA
(3) Department of Pathology, Cincinnati Children's Hospital Medical Center, Cincinnati, OH, USA

Email: Christy.Holland@uc.edu

ABSTRACT

Introduction: Cardiovascular disease is the number one cause of death worldwide and thrombo- occlusive disease is a leading cause of morbidity and mortality. Cardiovascular disease shares several risk factors with cancer and certain cancer treatments can increase the risk of subsequent cardiovascular disease. Ultrasound is both a valuable diagnostic tool and a promoter of beneficial tissue bioeffects for the treatment of cardiovascular disease. Vascular effects can be mediated by mechanical oscillations of circulating microbubbles that may co-encapsulate and shield therapeutic agents in the bloodstream. The effect of ultrasound on drug delivery was tested on two cardiovascular targets, intraluminal thrombus and atheroma in an *ex vivo* flow model using living porcine arteries.

Materials and Methods: Ultrasound-enhanced thrombolysis was investigated in two whole-blood clot models using a United States Food and Drug Administration-approved contrast agent (Definity, Lantheus Medical Imaging; Billerica, MA USA) and thrombolytic drug (recombinant tissue-type plasminogen activator [rt-PA]) (Genentech; South San Francisco, CA USA). Porcine venous blood was collected from donor hogs and coagulated in vials made of two different materials to produced retracted and unretracted clots, as determined by routine scanning electron microscopy and histology. Clots were deployed in an *ex vivo* porcine thrombosis model, and exposed to 3.15 µg/mL rt-PA and an intermittent 120 kHz ultrasound scheme previously developed to maximize stable cavitation while acoustic emissions were detected for 30 min. Clot mass loss was employed as a metric of thrombolytic efficacy. The effect of color-Doppler ultrasound exposure on bevacizumab-loaded liposome delivery into the vascular bed was also assessed in atheromatous porcine carotid arteries using the same *ex vivo* flow model. Bevacizumab, an anti-angiogenic antibody to vascular endothelial growth factor (VEGF-A), was loaded into echogenic liposomes (BEV-ELIP) and confirmed to be immunoreactive. BEV-ELIP flowing within the lumen were exposed to color-Doppler ultrasound at three acoustic pressures (0.00, 0.04, and 0.23 MPa) for 3.5 min during treatment at physiologic temperature and fluid pressure. To confirm the presence of bubble activity, cavitation was detected within the lumen by a single-element passive cavitation detector. After treatment, the artery was fixed at physiologic pressure and subjected to immunohistochemical analysis to assess the penetration of bevacizumab within the carotid wall.

Results and Discussion: Exposure to rt-PA promoted lysis in both clot models, compared with exposure to plasma alone. However, only unretracted clots experienced significant enhancement of rt-PA thrombolysis in the presence of Definity and ultrasound, compared with rt-PA alone. Microscopy revealed loose erythrocyte aggregates, a significantly less extensive fibrin network and a higher porosity, which may facilitate increased penetration of thrombolytics by cavitation. Regarding delivery of bevacizumab to atheromatous porcine arteries, other factors may more strongly influence the deposition of bevacizumab into carotid tissue than color-Doppler ultrasound and cavitation. In both sets of arteries, preferential accumulation of bevacizumab occurred in locations associated with atheroma progression and neointimal thickening: fibrous tissue, necrotic plaque and areas near macrophage infiltration. The delivery of bevacizumab to carotid vascular tissue correlated with the properties of the tissue bed, such as permeability, or affinity for growth-factor binding [Sutton *et al. Drug Delivery*, In Press 2016]. The authors acknowledge financial support from NIH R01 NS047603, R01 HL074002, and KL2 TR000078.

Keywords: Ultrasound-enhanced Thrombolysis, Drug Delivery, Stable Cavitation, Atherosclerosis, Bevacizumab

Detecting Tumour Response to a Vascular Disrupting Agent Using Multispectral Optoacoustic Tomography

Clinton W. Hupple (1), James Campbell (2), Jeni Gerberich (2), Mark D. Pagel (3), Ralph P. Mason (2), Julio Cárdenas-Rodríguez (3)

(1) iThera Medical GmbH, München, Germany
(2) Department of Radiology, UT Southwestern, Dallas, USA
(3) Department of Medical Imaging, University of Arizona, Tucson, USA

Email: Clinton.Hupple@ithera-medical.com

ABSTRACT

Introduction: Vascular disrupting agents (VDAs) are a promising class of drugs that selectively disrupt the tumor vasculature, and induce tumor necrosis by preventing the delivery of critical nutrients. CA4P is a VDA that has undergone extensive clinical trials and has been evaluated in pre-clinical studies using multiple modalities. Its effect on tumor vasculature and oxygenation has been assessed by MRI and bioluminescence imaging, but these methods are time consuming, complex and expensive. In this study we used Multispectral Optoacoustic Tomography (MSOT) to image the fraction (%) of hemoglobin (HbO2), the fraction of deoxyhemoglobin (Hb), and tumor perfusion (DCE MSOT) in mouse model of breast cancer before and after treatment with CA4P.

Materials and Methods: Five nude mice mice were implanted subcutaneously with MDA-MB-231 breast cancer cells, and imaged by MSOT at baseline and at 4 and 24 hours after administration of CA4P (120 mg/kg, intraperitoneally). Each image MSOT session consisted of: a) MultiSpectral Unmixing (MSP) from 700 to 900 nm in steps of 5 nm (41 wavelengths), b) Dynamic OA Imaging (DCE MSOT) after injection of Indocyanine green (ICG, CardioGreen™,~80 nanomoles/kg) performed by interleaving the acquisition of data after excitation at 800 nm (maximum for ICG) and 900 nm (control frequency) for 15 minutes. The MSP data was used to estimate the relative concentrations of Hb and HbO2, the DCE MSOT data was used to estimate the area under the curve after of the OA signal (AUC). The Kruskal Wallis test was used to test equal distributions between time points for Hb, HbO2, and AUC. This is the non-parametric equivalent of ANOVA.

Results and Discussion: All tumors showed lower HbO2 fractions and higher AUC that other tissues. Upon administration of CA4P, all tumors showed a ≥50 % decrease in HbO2 fraction ($p \leq 0.016$), and a similar decrease in their AUC of DCE MSOT ($p \leq 0.032$). After 24 hours, the HbO2, Hb, and AUC returned to their baseline levels ($p \geq 0.74$). The total hemoglobin was not significantly different among the three time points. These results are consistent with a decrease in perfusion after VDA administration.

Keywords: Optoacoustics, Photoacoustics, Oxygenation, Vascular Disrupting Agents, Tumour Response, Dynamic Contrast Enhancement

Implications of 'Vessel Co-option' by Tumors for Antiangiogenic Therapy of Metastatic Disease

Elizabeth Kuczynski (1), Andrew Reynolds (3), Robert S. Kerbel (1,2)

(1)) Biological Sciences Platform, Sunnybrook Research Institute, Toronto, ON, Canada, M4N 3M5
(2) Department of Medical Biophysics, University of Toronto, Toronto, ON, Canada, M4N 3M5
(3) Tumor Biology Team, The Institute of Cancer Research, London, UK SW3 6JB

Email: robert.kerbel@sri.utoronto.ca

ABSTRACT

Introduction: As of Oct. 2016 at least 10 different VEGF inhibiting antiangiogenic drugs have been approved for treatment of 8 types of overt advanced/metastatic cancer including colorectal, ovarian, cervical, renal, hepatocellular and non small cell lung carcinomas. However, the phase III trial successes that led to these approvals are offset somewhat by a number of limitations and failures, eg. only modest gains reported in PFS and OS, and failure thus far of all adjuvant antiangiogenic drug phase III trials. As a result, there has been a major effort to understand the basis of intrinsic or acquired resistance to such drugs. This effort includes developing improved preclinical cancer therapy models in mice since many preclinical studies preceding clinical development almost always showed highly encouraging results. Most such studies utilized treatment of established primary tumors – not the more challenging clinical circumstance of metastatic disease.

Materials and Methods: We have developed a number of models of postsurgical early stage micrometastatic or advanced metastatic disease, or locally advanced orthotopic disease, to test different cancer drugs including antiangiogenic agents.

Results and Discussion: Using these models we recapitulated several phase III clinical trial failures or limited successes of different antiangiogenic drugs, eg. in breast or hepatocellular carcinoma (HCC), respectively. The basis of resistance, intrinsic or acquired, respectively, surprisingly, in these aforementioned situations was assessed to be a lack of angiogenesis, eg. in lung metastases. Instead the tumors hijack the existing rich vasculature ("vessel co-option") or switch from relying on angiogenesis initially to vessel co-option, eg. in the liver during antiangiogenic (sorafenib) therapy of HCC. Vessel co- option was also found to be common in human lung metastases obtained from patients with four different types of cancer. A major question for the field is whether co-opted vessels, or the process of co-option, in tumors can be targeted by alternative 'anti-vascular' therapies independent of antiangiogenic drugs.

References:

Guerin, E., Man, S., Xu, P., and Kerbel, R.S. (2013) A model of postsurgical advanced metastatic breast cancer more accurately replicates the clinical efficacy of antiangiogenic drugs. **Cancer Res** *73*: 2743-2748.

Kuczynski, E.A., Yin, M., Bar-Zion, A., Lee, C.R., Butz, H., Man, S., Daley, F., Vermeulen, P.B., Yousef, G.M., Foster. F.S., Reynolds. A.R., and Kerbel, R.S. (2016) Co-option of liver vessels and not sprouting angiogenesis drives acquired sorafenib resistance in hepatocellular carcinoma. **J Nat'l Cancer Inst.**, *epub ahead of print*, Apr. 8.

Bridgeman, V.L., Vermeulen, P.B., Foo, S., Bilecz, A., Kostaras, E., Daley, F., Nathan, M., Wan, E., Frentzas, S., Schweiger, T., Hegedus, G., Renyi-Vamos, F., Vasudev, N., Larkin, J., Gore, M., Dvorak, H.F., Paku, S., Kerbel, R.S., Dome, B., and Reynolds, A.R. (2016) Vessel co-option is common in human lung metastases and mediates resistance to anti-angiogenic therapy in preclinical lung metastasis models. **J Path**, *in press.*

Keywords: Antiangiogenesis; VEGF; Drug Resistance; Metastasis; Vessel Co-option; Animal Models

On the Potential of Photoacoustic Tissue Characterization for Cancer Treatment Monitoring

Michael C. Kolios

Department of Physics, Ryerson University

Email: mkolios@ryerson.ca

ABSTRACT

Photoacoustic imaging (PAI) relies on generation of ultrasound waves from optically absorbing structures. The interest in PAI for biomedical applications has been growing and is possibly one of the most exciting new biomedical imaging techniques of this decade. PAI provides anatomical and functional information with excellent temporal and spatial resolution for specific applications. In a manner somewhat similar to B-mode imaging in ultrasound, most algorithms use only on the intensity of the detected photoacoustic waves for the image reconstruction. Methods developed in ultrasound tissue characterization have shown that sub-resolution structures can be inferred by analysis of the "raw" radiofrequency RF data. The ultrasound waves produced by the absorption of light in tissue can be analysed by these methods; in this case the interpretation of the analysis is based on the physics of photoacoustic wave generation. In the absence of exogenous absorbers, blood is one of the dominant optically absorbing tissues and hemoglobin in red blood cells (RBC) is the main endogenous chromophore. The spatial distribution of red blood cells in tissue determines the frequency content of the ultrasound signals produced. Analysis of the signals can reveal information related to the tissue vasculature and the functional state of the RBCs.

This information can be used in cancer treatment monitoring, especially for treatments that perturb the tumor vasculature. Moreover, tumor vessels are structurally different: they are torturous and typically hyperpermeable. Therapies that target the vasculature can induce changes in the vascular networks that in principle should be detected using photoacoustic imaging. In this presentation we will show how the frequency content of the photoacoustic signals encodes information about the size, concentration and spatial distribution of non-resolvable blood vessels that can be used to assess treatment response and speculate on how we can use photoacoustic imaging to guide drug delivery and monitor its effects on tissues.

Keywords: Photoacoustics, Cancer Treatment Monitoring

Luminal Water Imaging – a Novel Quantitative MRI Technique for Prostate Cancer Diagnosis

Piotr Kozlowski (1,2,3,5), Shirin Sabouri (1), Silvia Chang (2), Edward Jones (4), Ladan Fazli (5), Larry Goldenberg (4,5)

(1) UBC MRI Research Centre, UBC Departments of (2) Radiology, (3) Urologic Sciences, and (4) Pathology and Laboratory Medicine, (5) Vancouver Prostate Centre, Vancouver, BC, CANADA

Email: Piotr.Kozlowski@ubc.ca

ABSTRACT

Introduction: Prostate cancer remains the most common noncutaneous malignancy in North American males and second leading cause of cancer related deaths in men. Owing to the widespread use of screening tests, many more prostate tumours are being detected, many of which are less advanced, localized, lower risk cancers. This prompted increased interest in focal therapy as an alternative to the traditional therapies of radical prostatectomy and radiation therapy. The ultimate success of focal therapy relies on proper patient selection and adequate characterization of the tumour's location, extend, and histological grade. We present a novel MRI technique, based on multi-component T2 measurements, for prostate tumour detection and grading.

Materials and Methods: Quantitative T2 measurements were carried out in 18 prostate cancer patients on a 3T MRI scanner (Philips, The Netherlands), using a multi-echo GRASE sequence. Continuous T2 distributions were calculated for each pixel from the multi-echo data using a regularized non-negative least squares (NNLS) analysis. A novel parameter, called Luminal Water Fraction (LWF), was calculated as a ratio of the area under the long T2 peak (corresponding to luminal water inside the glands) divided by the integral of the entire T2 distribution. MRI results were correlated with histology of the whole-mount sections following prostatectomy.

Results and Discussion: Luminal Water Fraction was significantly smaller in cancerous than in normal tissue, both in the Peripheral Zone (PZ): 0.1 vs. 0.22, $p < 0.0001$, and the Central Gland (CG): 0.08 vs. 0.2, $p < 0.0001$. LWF values strongly correlated with the Gleason score: rho = -0.749, $p < 0.0001$ in PZ, and rho = -0.646, $p < 0.0001$ in CG. Receiver Operating Characteristic analysis showed the Area Under Curve (AUC) values of 0.93 ($p < 0.0001$) for PZ and 0.91 ($p < 0.0001$) for CG. LWF values were strongly correlated with the percentage area of luminal space assessed with histology: rho = 0.75, $p<0.0001$.
Our preliminary results show that the LWF, a novel parameter calculated from the multi-echo T2-decay data, can distinguish between normal and cancerous tissue, and strongly correlates with the Gleason score. The ROC analysis showed AUC values higher than typically achievable with multi-parametric MRI examinations. Thus, considering that the multi-echo data were acquired in just over 11 minutes, our results strongly suggest that this novel approach may be more advantages for prostate cancer detection and staging, than currently used techniques.
Our results also demonstrate that LWF is significantly correlated with the percentage area of luminal space in the prostatic tissue, and thus can be useful in diagnosing various prostatic diseases, in which the amounts of lumen differs between normal and abnormal tissues.

Acknowledgements: This study was supported by the Canadian Institutes of Health Research.

Keywords: Prostate Cancer, Quantitative MRI, Multi-Component T2, Gleason Score, Histology

Microbubbles for Cavitation Enhanced Treatment
Non-Invasive Tissue Reduction for Treatment of Hypertrophic Cardiomyopathy

Oliver D. Kripfgans (1), Xiaofang Lu (1), Chunyan Dou (1), Yiying I. Zhu (1), Mario L. Fabiilli (1), Gabe E. Owens (2), William Armstrong (3), Douglas L. Miller (1)

(1) Department of Radiology, University of Michigan, Ann Arbor, MI, 48109, USA
(2) Department of Pediatrics and Communicable Diseases, University of Michigan, Ann Arbor, MI, 48109, USA
(3) Department of Internal Medicine - Cardiology, University of Michigan, Ann Arbor, MI, 48109, USA

Email: oliver.kripfgans@umich.edu

ABSTRACT

Introduction: Hypertrophic cardiomyopathy (HCM) a common genetic cardiovascular disease, occurring in 1 in 500 people. Patients may experience shortness of breath, angina and palpitations, but for some the first sign is sudden death. Septal hypertrophy leads to obstruction of the left ventricular outflow path in up to 75% of patients. About one-third of patients with obstruction remain symptomatic after pharmacological therapy and are candidates for tissue debulking. Two available methods are open-heart surgery for septal myectomy and transcatheter septal ablation with alcohol. The less invasive alcohol ablation procedure unfortunately produces a high incidence of heart block requiring pacemaker placement and has a high incidence of arrhythmia and thus is not widely applied. A completely new and non-invasive option for myocardial tissue reduction is sorely needed. The objective of this work is to create a safer, gentler method of cardiac tissue reduction for HCM and other hypertrophies.

Materials and Methods: Myocardial contrast echocardiography (MCE) has enabled visualization of myocardial perfusion. High Mechanical Index MCE in rats causing intermittent destruction of contrast microbubbles in the myocardium has been shown to lethally injure cardiomyocytes by acoustic cavitation. This phenomenon leads to randomly scattered microlesions involving one or a few cardiomyocytes throughout the targeted myocardium. Animal procedures were conducted with approval and guidance of the Institutional Animal Care and Use Committee. One year old, purpose bread salt sensitive brown Norwegian (SS/BN) rats (University of Wisconsin) were used as an in vivo model for HCM. Under ketamine/xylazine IP anesthesia, contrast agent was infused at a rate of 5 µL/min/kg into a tail vein catheter. A cardiac phased array (10S, Vivid 7, GE Healthcare) was coupled to the shaved and depilated left thorax and the left ventricular myocardium visualized. In this arrangement a 19 mm diameter single element therapy transducer was co-aligned to aim at a registered region of interest in the field of view of the 10S array. For therapy, 10-cycle tone bursts at 1.5 MHz, 4 repetitions at 0.25 ms pulse interval (*i.e.* 4.0 kHz PRF) were spaced every 8 heartbeats and triggered at end systole (RR/3, using ECG gating) to allow microbubble refill after cavitation. Peak negative free field pressures of 4 MPa were used to intermittently induce cavitation for 10 min. Troponin levels were measured 4 h after treatment.

Results and Discussion: Myocardial wall thickness as measured by echocardiography, was reduced from an average of 2.09±0.15 mm before treatment to 1.80±0.29 mm at 4 weeks post treatment. This is a 16% reduction with a p-value of 0.004 relative to the sham group, which measured 2.07±0.11 mm and 2.12±0.10 mm before and after treatment. For troponin levels >10 ng/mL and >90% PVC during treatment a reduction of 22% was seen, while troponin levels <10 ng/mL and <90% PVC, resulted only in a 2% reduction, as measured by echocardiography. Histological analysis revealed a myocardial thickness of 1.39 and 1.80 mm for treated and sham, respectively, *i.e.* a 23% reduction. Cavitation enhanced therapy maybe a possible avenue for non-invasive tissue reduction for treatment of hypertrophic cardiomyopathy and echocardiography can be an adequate tool to estimate tissue reduction in rodents. ECG and troponin may be suitable as a real-time and short-term feedback for therapy efficacy.

Keywords: Ultrasound Contrast Agent, Cavitation, Hypertrophic Cardiomyopathy, Ablation

Picosecond Cell Nanosurgery using Gold Nanoparticle Assemblies

Yevgeniy R. Davletshin (1), J. Carl Kumaradas (1)

(1) Ryerson University, Department of Physics, Toronto, Ontario, Canada, M5B 2K3

Email: ckumarad@ryerson.ca

ABSTRACT

Introduction: Laser induced optical breakdown (LIOB) in the vicinity of gold nanoparticles is an area of an active research. In addition to optoporation, it is being studied for applications in many areas in medicine and biology, such as nanoparticle enhanced LIOB spectroscopy, cell nanosurgery and drug release. Such a broad range of applications stems from the gold nanoparticles' unique optical properties in the visible and near-infrared wavelengths, where biological tissues are most transparent to incoming laser irradiation. The interaction of light with a gold nanoparticle induces a localized surface plasmon resonance (LSPR), where the oscillation of quasi-free electrons along the gold nanoparticle's surface produces a near-field enhancement of the incident radiation. The spectral characteristics of LSPR are highly dependent on the nanoparticle morphology (shape/size/composition), aggregation, dielectric properties of the external environment.

Nanoparticle-mediated optical breakdown is a complex process due to the large variety of parameters involved, such as laser source characteristics (fluence/wavelength/pulse duration) and nanoparticle morphology (size/shape/composition). Therefore, the optimization and control of a nanoparticle-mediated optical breakdown threshold is challenging. Computational analysis can be used to model the optical breakdown process and to obtain insight into the LIOB process. Although the computational modelling of nanoparticle-mediated LIOB is difficult, there are many unanswered questions, such as how the optical properties of the nanoparticle are influenced by its local environment, and how the threshold of LIOB depends on morphology of the nanoparticle and laser parameters, that motivate the development of numerical models.

Materials and Methods: We have developed a theoretical model of nanoparticle-mediated LIOB to study the nanoparticle morphology dependence of the optical breakdown threshold during picosecond pulse exposure. This was done using the finite element analysis software – COMSOL Multiphyiscs. Theoretical model was used to study an on- and off-resonance 6 ps laser pulse interactions with uncoupled and tightly-coupled gold nanospheres and nanorod monomers of different sizes, with a focus on the thermal and optical processes.

Results and Discussion: The study shows that the optical breakdown threshold for picosecond-pulse interaction with uncoupled and tightly-coupled gold nanoparticles of different morphologies is highly dependent on the near-field enhancement in the vicinity of the nanoparticle and to a lesser degree on type, volume and absorption cross-section of the nanoparticle.

Keywords: Gold Nanoparticle, Nanorod, Nanosphere, Optical Breakdown, Finite Element Analysis

Opportunities for Rapid MRI in Radiation Oncology

Angus Z. Lau (1,2)

(1) Physical Sciences, Sunnybrook Health Sciences Centre, Toronto, ON, Canada, M4N 3M5
(2) Medical Biophysics, University of Toronto, Toronto, ON, Canada, M4N 3M5

Email: angus.lau@sri.utoronto.ca

ABSTRACT

Introduction: The development of the MRI-LINAC, a combined MRI / radiation therapy hybrid device, offers opportunity for novel uses of MRI in radiation oncology. Adaptive treatment, motion management, and rapid assessment of treatment response are important applications of this new technology. Clinical adoption of the MRI-LINAC will require optimized protocols with short scan times to maximize the information acquired.Recent advances in MRI data acquisition provide order-of-magnitude reductions in scan time. This translates into higher throughput scans, improved image quality, and better spatial coverage.

We will discuss recent results in cardiac diffusion tensor imaging (DTI), an MRI scan used to characterize the microstructure of the heart. Impairments in cardiac fibre structure are implicated in development of cardiac arrhythmias and sudden cardiac death. However, DTI is associated with long scan times,which limit the patient population that can benefit from this exam.We will discuss acceleration using simultaneous multi-slice (SMS) excitation for cardiac DTI, and its potential application in radiation oncology.

Materials and Methods: SMS excitation was incorporated into a cardiac DTI pulse sequence and implemented on a Siemens 3T scanner. Image quality (SNR, andvarious diffusion metrics) was compared between a conventional single-slice scan taking 9 breath-holds, and an accelerated 3-slice scan in the same scan time.

Results and Discussion: No significant difference was observed in diffusion parameters between a time-equivalent conventional single-slice scan, and a three-fold accelerated SMS acquisition. The accelerated sequence reduces the number of breath-holds required for a 3-slice scan to 9 (from 27), making it practical to incorporate DTI measurements within a comprehensive cardiac exam. We anticipate that this strategy will be broadly applicable in MR-guided radiation oncology.

Keywords: Imaging, MRI, Radiation Therapy, Adaptive Treatment, Response

Alpinion Clinical Research Ultrasound System

Julian Lee (1)

(1) Alpinion Medical Systems, USA

Email: julian.lee@alpinionusa.com

ABSTRACT

Introduction: ALPINION MEDICAL SYSTEMS is dedicated to developing and producing ultrasound research platform, E-CUBE 12R (FDA 510K clearance) which combines a premium clinical system and research platform. With its innovative beamforming technology, open software based platform and fast frame rate, the E-CUBE 12R allows researchers to access full channel RF data, to build sequence control, and to create more valuable clinical studies such as photoacoustics, Elastography, drug delivery contrast agent imaging and many of translational research.

Key Features of E-CUBE 12R:
›› Research Platform with Clinical Scanning Capability(FDA 510K)
›› Open Software Based Platform and Sequence Control
›› Software Beamforming
›› Acoustic Radiation Force Impulse (ARFI) Control
›› Realtime RF Channel Data Access Without Additional Hardware
›› Plane Wave Imaging / Fast Frame Rate Imaging (up to 9,000 fps)
›› Realtime Dual Display (ex. Focused and Planewave) using Dual TX/RX Paths

Keywords: Research Ultrasound, Planewave Imaging, Shearwave Imaging, ARFI, Channel Data

Nonlinear Ultrasound Parameters to Monitor Mitotic Catastrophe or Apoptosis in Cell Pellet Biophantoms

Pauline Muleki-Seya (1), Cedric Payan (1), Laure Balasse (2), Sara Karaki (3), Regine Guillermin (1), Sandrine Roffino (4), Palma Rocchi (3), Benjamin Guillet (2), Emilie Franceschini (1)

(1) Aix Marseille Univ, CNRS, Centrale Marseille, LMA, Marseille, France
(2) Aix Marseille Univ, INSERM, VRCM, Marseille, France
(3) Aix Marseille Univ, CNRS, INSERM, Institut Paoli-Calmettes, CRCM, Marseille, France
(4) Aix Marseille Univ, CNRS, ISM, Marseille, France
(a) Present address: Bioacoustics Research Laboratory, Department of Electrical and Computer Engineering, University of Illinois at Urbana-Champaign, 405 N. Mathews, Urbana, IL 61801

Email: pauline.muleki@gmail.com

ABSTRACT

Introduction: Cell death induced by chemotherapy, whether by apoptosis or mitotic catastrophe, come along with important cell morphologic modifications. During apoptosis, cell shrinkage as well as condensation and fragmentation of the nucleus occur, whereas multinucleated and swelling cells are observed during mitotic catastrophe. This evolution in cell morphology could lead to modification of the nonlinear ultrasound component in the backscattering signal. In this study, we investigate the behavior of such nonlinear parameters as biomarkers to monitor anticancer therapy (cell apoptosis and mitotic catastrophe).

Materials and Methods: PC3 cells have been treated with 100 nM of docetaxel (inducing mitotic catastrophe and apoptosis) for different treatment times between 6h to 48h hours. HT29 cells have been treated for 24h with different doses of staurosporine (inducing cell apoptosis) and treated with 0.50 µM for different treatment times between 6h to 48h hours. Flow cytometry analysis was performed on cell samples to measure cell DNA content and to quantify cell death. Ultrasound measurements were performed on centrifuged cells to form a packed cell pellet using a Vevo 770 high frequency ultrasound system with RMV710 (F_c: 20 MHz) and RMV703 (F_c: 30 MHz) probes. For each cell pellet, backscattered signals were acquired in two regions of interest for different powers of excitation of the ultrasound system: 5, 10, 20, 40, 50, 63 and 100%. Nonlinear parameters were obtained from the Subtraction Scaling Method (SSM) on the spectrum of backscattered signals. We assume that the medium is (acoustically) linear when sonicated by the lower power of excitation (i.e. 5%). A power law fit is performed on the linear energy versus nonlinear energy for the different powers and two parameters are estimated: the exponent of the power law α and the nonlinear energy at a fixed linear energy value I_{NL}.

Results and Discussion: The PC3 cells treated with docetaxel showed morphological modifications on the histological sections: larger cells, multinuclear cells with or without vacuoles. The nonlinear parameter α increases with treatment duration up to 24h, then decreases with treatment duration (with RMV703 probe). The parameter α is quite well correlated with percentage of cells with vacuoles (R_2=0.68) and the percentage of early apoptosis (R_2=0.63). The HT29 cells treated with staurosporine showed cell apoptosis. The nonlinear parameter I_{NL} decreases with drug dose and with treatment duration (with RMV703 probe). The parameter I_{NL} is quite well correlated with the percentage of apoptotic cells (R_2=0.59).

Keywords: Ultrasound Scattering, Nonlinear Acoustics, Cell Pellet, Apoptosis, Mitotic Catastrophe

Quantitative Ultrasound: Some Interesting Outcomes

William D. O'Brien, Jr.

Bioacoustics Research Laboratory, Department of Electrical and Computer Engineering, University of Illinois, 405 N. Mathews, Urbana, IL 61801 USA

Email: wdo@uiuc.edu

ABSTRACT

Introduction: The objective of soft tissue quantitative ultrasound (QUS) is to improve diagnostic ultrasound imaging via quantitative outcomes. The quantitative components of ultrasound (attenuation and backscatter) are showing sensitivity to inflammatory processes, thereby making QUS capable for detection and grading such morphological conditions. But inflammation is not the whole story; the key is to identify the ultrasonic scattering causes of the inflammatory processes. Two specific induced conditions are examined, viz., cell pellets undergoing known apoptosis and pancreases undergoing pancreatitis for which temporally the ultrasonic attenuation coefficient (AC: dB/cm-MHz) and backscatter coefficient (BSC: 1/cm-sr) are quantified.

Materials and Methods: The AC and BSC (20-50 MHz) are estimated for cell pellets ex vivo and Sprague-Dawley rats pancreases in vivo and ex vivo. Various cell types are subjected to doxorubicin (control [no dox], and 24 and 48 hours) to promote apoptosis. The rats are subjected to cerulein (control [no cerulein], and between 4 and 168 hours) to promote pancreatitis, and mimic certain morphologic similarities of pancreatic carcinoma.

Results and Discussion: The AC and BSC of the cell pellet study showed distinct and measureable differences between the control and the doxorubicin-induced apoptosis. Likewise, the AC and BSC of the pancreas study showed distinct and measureable differences between the control and the cerulein-induced pancreatitis. Both studies are providing valuable information for detecting and grading certain aspects of cancer. (NIH Grant R37EB002641)

Keywords: Quantitative Ultrasound, Attenuation Coefficient, Backscatter Coefficient, Doxorubicin, Apoptosis, Cerulein, Pancreatitis.

The Potential of Monitoring of Focused Ultrasound Treatment of Solid Tumors using Quantitative Ultrasound

Michael L Oelze, Jeremy Kemmerer, Rita J Miller, Goutam Ghoshal

Bioacoustics Research Laboratory, Department of Electrical and Computer Engineering, University of Illinois at Urbana-Champaign, Urbana, IL, USA 61801

Email: Oelze@illinois.edu

ABSTRACT

Introduction: The success of any minimally invasive treatment procedure can be enhanced significantly if combined with a robust noninvasive imaging modality that can monitor therapy in real time. Quantitative ultrasound (QUS) imaging has been widely investigated for monitoring various treatment responses such as chemotherapy, radiation and thermal therapy. We demonstrate that QUS has the potential to be used to monitor in real time the treatment of solid tumors using high intensity focused ultrasound (HIFU) to heat tumors in rats.

Materials and Methods: In the studies we examined the use of spectral-based QUS parameters to monitor HIFU treatment of *ex vivo* rat mammary tumors and *in vivo* rat mammary adenocarcinoma tumors (MAT) where significant tissue motion was present. HIFU was applied to tumors in rats using a single-element transducer. During the off part of the HIFU duty cycle, ultrasound backscatter was recorded from the tumors using a linear array co-aligned with the HIFU focus. Spectral parameters from the backscatter coefficient, i.e., effective scatterer diameter (*ESD*) and effective acoustic concentration (*EAC*), were estimated during treatment. The changes of each parameter during treatment were compared with a temperature profile recorded by a fine needle thermocouple inserted into the tumor a few millimeters behind the focus of both the HIFU and the imaging transducer array.

Results and Discussion: In the in vivo case, the mean *ESD* changed from 121±6 μm to 81±8 μm (*p*–value = 0.0002), and the *EAC* changed from 33±2 dB/cm^3 to 46±3 dB/cm^3 (*p*–value = 0.0002) during HIFU exposure as the temperature increased on average from 38.7±1.0°C to 64.2±2.7 °C. The changes in *ESD* and *EAC* were linearly correlated with the changes in tissue temperature during the treatment. When HIFU was turned off, the *ESD* increased from 81±8 μm to 121±7 μm and the *EAC* dropped from 46±3 dB/cm^3 to 36±2 dB/cm^3 as the temperature decreased from 64.2±2.7 °C to 45±2.7 °C. QUS was demonstrated both *ex vivo* and *in vivo* to track temperature elevations caused by HIFU exposure.

Keywords: Quantitative Ultrasound, High Intensity Focused Ultrasound, Focus Ultrasound, Thermometry

Ultrasound-Mediated Drug Delivery for the Treatment of Leptomeningeal Metastases

Meaghan A. O'Reilly (1,2), My-Linh Yee (1), Sheng-Kai Wu (1), KullervoHynynen (1,2), Robert Kerbel (2,3), Gregory J. Czarnota (1,2,4,5), Kathleen Pritchard (6,7), Arjun Sahgal (1,4,5)

(1) Physical Sciences, Sunnybrook Research Institute, Toronto, ON, Canada, M4N 3M5
(2) Department of Medical Biophysics, University of Toronto, Toronto, ON, Canada, M4N 3M5
(3) Biological Sciences, Sunnybrook Research Institute, Toronto, ON, Canada, M4N 3M5
(4) Radiation Oncology, Sunnybrook Health Sciences Centre, Toronto, ON, Canada, M4N 3M5
(5) Department of Radiation Oncology, University of Toronto, Toronto, ON, Canada
(6) Medical Oncology, Sunnybrook Health Sciences Centre, Toronto, ON, Canada, M4N 3M5
(7) Department of Medicine, University of Toronto, Toronto, ON, Canada

Email: moreilly@sri.utoronto.ca

ABSTRACT

Introduction: Leptomeningeal metastases (LM), the metastatic involvement of the meninges lining the brain and spinal cord, is a late metastatic complication with a median survival of ~4.5 months from diagnosis. The presence of the barriers of the CNS (Blood-Brain, Blood-Spinal Cord and Blood-CSF barriers) make these lesions difficult to treat with drug therapies. Ultrasound (US) has been shown to permeabilize the Blood-Brain barrier (BBB) and Blood-Spinal Cord barrier (BSCB) to facilitate drug delivery. The objective of this work is to investigate the potential of US-mediated drug delivery in improving the outcome of LM.

Materials and Methods: Athymic rats (n=10) underwent laminectomy at L4 followed by catheterization of the subarachnoid space. 7 days following surgery, HER2 expressing human breast cancer cells were injected into the catheter to induce the tumor. The animals were imaged on a 7T MRI weekly beginning d6 post-implantation. At the first detection of bulk LM deposits the animals were assigned to 1 of 3 groups: control (n=2), trastuzumab (Herceptin) only (n=4) or trastuzumab + US (n=4). Animals receiving trastuzumab (intravenously administered) were treated weekly for three weeks beginning with a loading dose of 8mg/kg in the first week, followed by a maintenance dose of 6mg/kg in subsequent weeks. In the trastuzumab + US group the BSCB was opened using US (551.5 kHz, 10ms bursts, 1 Hz PRF) and Definity microbubbles under MRI guidance. The US pressures were actively controlled based on the signals from the microbubbles, as has been previously described for the brain [O'Reilly and Hynynen, *Radiology*, 2012].

Results and Discussion: Bulk LM deposits appeared between d13 and d28 post-implantation, (median = d21). Tumor growth, as assessed by contrast MRI, was suppressed in the US + drug group vs the drug alone group. On histology, a significant difference ($p = 0.04$) in tumor burden was observed between animals in the drug only group (mean tumor volume = 33 ± 15 mm^3) compared with the US + drug group (9 ± 6 mm^3). The results show promise for the use of ultrasound in the treatment of leptomeningeal metastases. Future studies will extend this preliminary work to larger, fully controlled cohorts.

Keywords: Ultrasound, Drug Delivery, Spinal Cord, Leptomeningeal Metastases

Cavitation-Enhanced Ultrasound-Mediated Tumor Ablation Nucleated with Phase-Shift Nanoemulsions

Calum Crake (1), Jason Papademetriou (2), Yongzhi Zhang (1), Nathan McDannold (1), Tyrone Porter (2,3)

(1) Department of Radiology, Brigham & Women's Hospital/Harvard Medical School, Boston, MA
(2) Department of Mechanical Engineering, Boston University, Boston, MA
(3) Department of Biomedical Engineering, Boston University, Boston, MA

Email: tmp@bu.edu

ABSTRACT

Introduction: Ultrasound-mediated thermal ablation has proven to be an effective strategy for treating solid tumors. However, the acoustic power and exposure times required can be excessive. It is well documented that cavitation can accelerate ultrasound-mediated heating and dramatically reduce the acoustic power required. In this study, vaporizable perfluorocarbon nanoemulsions were used to nucleate cavitation directly in solid tumors and MR thermometry and passive cavitation mapping were utilized to monitor cavitation-enhanced heating and tumor ablation.

Materials and Methods: VX2 tumors were established in the hind limb of rabbits. The tumor was positioned within an MR imaging coil and at the focal point of an MR-compatible focused ultrasound transducer. A linear array connected with a Verasonics system was positioned such that the tumor was in its imaging plane. Lipid-coated phase-shift nanoemulsions (PSNE) were injected intravenously and allowed to accumulate within solid tumors. High power acoustic pulses were used to vaporize the PSNE directly in the tumor and induce cavitation-enhanced heating. Thermal maps were generated via MR thermometry and cavitation maps were generated via the passive cavitation detection system. The spatial correlation of the thermal and cavitation maps were examined and thermal and cavitation dose as functions of time were estimated. Lastly, tumors were harvested and the ablated volume was evaluated via histology.

Results and Discussion: Evidence of PSNE vaporization and sustained cavitation was acquired using the passive cavitation mapping system. Accelerated heating detected with MR thermometry correlated well with the initiation of cavitation both temporally and spatially. In tumors where PSNE were vaporized, the thermal dose required for ablation was achieved at a lower power and shorter exposure time compared to tumors where PSNE was not vaporized. Evidence of coagulative necrosis associated with thermal ablation was detected in histological sections. The results demonstrate that local cavitation can be nucleated with PSNE in solid tumors and subsequent cavitation activity and ultrasound-induced heating can be monitored concurrently. The technique may be leveraged to enhance ultrasound-induced ablation of solid tumors, particularly in highly vascularized organs.

Keywords: Perfluorocarbon Nanoemulsions, Nanodroplets, Cavitation, Thermal Ablation

Prostate-Cancer Imaging at High Frequencies using Quantitative Micro-Ultrasound

Daniel Rohrbach (1), Brian Wodlinger (2), Jerrold Wen (2), Jonathan Mamou (1), Ernest Feleppa (1)

(1) Lizzi Center for Biomedical Engineering, Riverside Research, New York, NY, USA, 10038
(2) Exact Imaging, Markham, Ontario, Canada

Email: drohrbach@RiversideResearch.org

ABSTRACT

Introduction: Currently, the only method for definitive diagnosis of prostate cancer is via biopsies guided by transrectal ultrasound (TRUS). Previous studies by our group suggested that quantitative ultrasound (QUS) could provide a more-sensitive and more-specific means of targeting biopsies to cancer-suspicious regions in the prostate. Such a tool would reduce current high numbers of false-negative diagnoses and unnecessary biopsies. The previous studies utilized ultrasound signals at typical clinical frequencies, i.e., in the 6-MHz range. In the current study, we investigate the potential of incorporating our QUS approaches in a novel micro-ultrasound scanner operating at high frequencies for identifying cancerous regions in the prostate

Materials and Methods: A 29-MHz, transrectal, micro-ultrasound system and transducer (ExactVu™ micro-ultrasound, Exact Imaging, Markham, Canada) was used to acquire RF data from 16 patients directly before 12-core biopsy (192 cores total). These retrospective data are a subset of data acquired in an ongoing, multisite, 2,000- patient, randomized, clinical trial (clinicaltrials.gov NCT02079025). For each RF data set, normalized power spectra were computed along the biopsy needle trace located inside the prostate using a sliding region of interest (ROI) of approximately 1 mm^2 in size. Spectra from the set of ROIs, were averaged and normalized by a reference spectrum obtained from a calibration phantom consisting of 18-µm polystyrene beads. QUS estimates of midband (M), intercept (I) and slope (S) were calculated and used to train linear discriminant classifiers (LDCs). Classifier performance was assessed using area-under-the-curve (AUC) values obtained from receiver operating characteristic (ROC) analyses with leave-one-out cross validation.

Results and Discussion: A combination of S and I resulted in an AUC value of 0.74. When PSA value was added as a feature the AUC increased to 0.79. In a previous study, a protocol for prostate-cancer risk identification using micro- ultrasound (PRI-MUS™) was introduced for the ExactVu™ system to provide a subjective, user- dependent, B-mode-based scoring system for assessing prostate-cancer likelihood. The B-mode-based study demonstrated a peak AUC of 0.74 for higher GS values (GS > 7) when read by an expert. Our initial results with AUC values of 0.79 are very encouraging for developing a new, entirely objective, prostate- cancer, risk-assessing tool. Currently, we are testing QUS approaches involving additional estimates (e.g. envelope statistics), and non-linear classifiers, such as support-vector machines, to improve classification performance. Figure 1 shows two example with classification scores obtained from LDC using I,S and PSA.

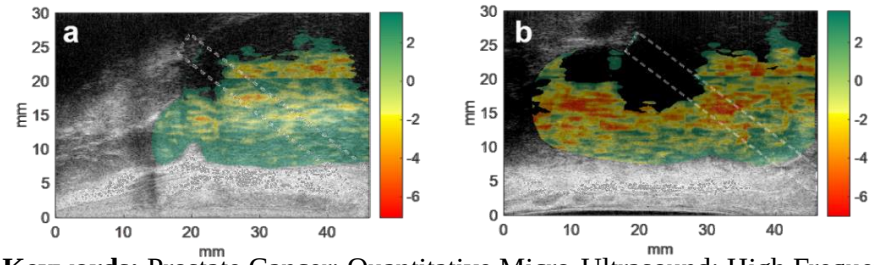

Figure 1 LDC *score overlaid on B-mode image of benign (a) and cancerous (b) prostate. Red indicates high cancer likelihood*

Keywords: Prostate Cancer; Quantitative Micro-Ultrasound; High Frequency; 29 MHz

Imaging-Based Analysis of Intratumour Heterogeneity for Monitoring Response to Anticancer Therapies

Ali Sadeghi-Naini (1,2,3,4), Lakshmanan Sannachi (1,2,3,4), Hadi Tadayyon (1,2,3,4), William Tran (1,2), Martin Stanisz (1,2), Harini Suraweera (1,2), Gregory J. Czarnota (1,2,3,4)

(1) Physical Sciences, Sunnybrook Research Institute, Sunnybrook Health Sciences Centre, Toronto, ON, Canada, M4N 3M5
(2) Radiation Oncology, Odette Cancer Centre, Sunnybrook Health Sciences Centre, Toronto, ON, Canada, M4N 3M5
(3) Department of Medical Biophysics, University of Toronto, Toronto, ON, Canada, M4N 3M5
(4) Department of Radiation Oncology, University of Toronto, Toronto, ON, Canada, M4N 3M5

Email: ali.sadeghi@sri.utoronto.ca

ABSTRACT

Introduction: Tumour response to anti-cancer therapies is often a gradual process that affects tissue micro-structure and physiology heterogeneously. Quantitative ultrasound and diffuse optical parametric imaging have demonstrated capable of characterizing response-related properties of tumour in terms of micro-structure, physiology and metabolism. As such alterations in textural features of these parametric maps, that quantify intratumour heterogeneity from various response-related perspectives, can potentially be applied to detect response to cancer-targeting therapies. In a series of studies, we investigated the efficacy of these imaging biomarkers to evaluate response to anticancer therapies early following the start of a treatment.

Materials and Methods: Experiments were conducted using animal tumour models receiving chemo or radiation therapy, and evaluated at different times after treatment using quantitative ultrasound parametric imaging. Tumours were excised immediately after scans and histology and immunohistochemistry were performed on tumour sections to quantify cell death. Observational clinical studies were carried out on locally advanced breast cancer patients receiving neo-adjuvant chemotherapy. Patients were scanned with clinical ultrasound and optical scanners prior to and at different times after the start of chemotherapy. Pathological response of patients were obtained after the surgery using whole-mount histopathology on mastectomy tumour sections. Patients were also followed up after their treatment and their clinical data were recorded for survival studies.

Results and Discussion: Results obtained from animal experiments demonstrated that, compared to average-based mean-value parameters, texture-based measures of tumour homogeneity derived from quantitative ultrasound parametric images are more sensitive to changes introduced within tumour in response to treatment. The textural features could detect lesser amounts of cell death early after treatment initiation and demonstrated higher levels of correlation to histological cell death. In the clinical studies, changes in textural features became apparent within one weeks after the start of chemotherapy in both quantitative ultrasound and optical parametric images. The textural parameters could predict the pathological response of patients to chemotherapy earlier after the start of treatment (at week 1) compared to the mean-value parameters (at weeks 4 and 8 of treatment), with high sensitivity and specificity. The patients classified as responders/non-responders using these textural biomarkers demonstrated significantly different survivals with a good agreement with those obtained based on pathology. The obtained results suggest that these imaging-based textural biomarkers, as early survival-linked surrogates of treatment response, may be applied to facilitate switching an inefficient treatment regimen to a more effective one on an individual patient basis, within days after the therapy initiation.

Keywords: Intratumour Heterogeneity, Textural Analysis, Quantitative Ultrasound, Optical Imaging, Treatment Response Monitoring

MRI of Cancer Therapies

Hatef Mehrabian, Kim Desmond, Wilfred Lam, Greg J. Stanisz

(1) Physical Sciences, Sunnybrook Research Institute, Toronto, ON, Canada, M4N 3M5
(2) Departments of Medical Biophysics, University of Toronto, Toronto, ON, Canada, M4N 3M5

Email: stanisz@sri.utoronto.ca

ABSTRACT

Introduction: The use of radiation therapy for the treatment of patients with solid tumours has been a standard clinical practice. Reliable biomarkers which allow for expeditious assessment of tumour response to radiation therapy are highly sought-after. Multiple treatment options are available, however, they require an early assessment of tumour response in order to switch the treatment while still within an effective time window. Current clinical practice is subjective, and relies heavily on the RECIST criteria which judge response by the largest intra-tumoral distance. This is inadequate for describing early apoptotic changes in cell structure which precede changes in tumour dimension that may not stabilize until weeks or months after treatment. Tumour biopsy may be informative, but is often too invasive, especially in the brain, and not completely descriptive of a heterogeneous tumour with a heterogeneous response. Managing radiation-induced late effects is also challenging, as high radiation doses increase the likelihood of developing necrosis which occurs months after treatment. It is difficult to differentiate radiation-induced changes from tumour progression using conventional MRI since they both appear as an enlarging enhancing region on post-Gadolinium (Gd) T1-weighted MRI, and as increased vasogenic edema on T2w-FLAIR.

Materials and Methods: We discuss the use of two quantitative MRI methods: Chemical Exchange Saturation Transfer (CEST) to assess tumour metabolism and Dynamic-Contrast-Enhanced MRI (DCE-MRI) to evaluate vascular and intra-extracellular cellular structure. The study was performed on a clinical 3T MRI system (Phillips) in 30 patients undergoing stereotactic radiosurgery (SRS) for brain metastasis. The patients were scanned before the SRS treatment and one and four weeks after.

Results and Discussion:
We were able to show that:

1. Quantitative assessment of changes in tumour metabolism (using CEST), and changes in tumour cellular microstructure as measured by intra-extracellular water exchange, were able to **separate responders from non-responders** one-week post treatment.
2. Quantitative MRI (qMRI) could also **predict, one week after treatment,** how much shrinkage of the original tumour mass may occur after one month.
3. Certain quantitative features of CEST (most notably Nuclear Overhauser Effect) could predict the tumour response **before treatment was administered**. This has significant implications, as the current model of "one size fits all", where tumours are given the same dose of radiation, can be changed to a radiation dosing scheme based on pretreatment CEST features of the tumour (Appendix 1).
4. CEST was capable of differentiating radiation necrosis from tumor progression in brain metastases.

Keywords: Chemical Exchange Saturation Transfer, SRS, tumour response, Brain Metastasis

Predicting Clinical and Pathological Response of Breast Tumours to Neoadjuvant Chemotherapy Using Pre-Treatment Textural Features of Diffuse Optical Spectroscopic Images

William Tyler Tran (1,2,3), Ali Sadeghi-Naini (1,2), Lee Chin (1), Lakshmanan Sannachi (1,2), Elyse Watkins (1), Sharon Lemon Wong (1), Belinda Curpen (1,2), Maureen Trudeau (1,2), Sonal Gandhi (1,2), Martin Yaffe (1), Elzbieta Slodkowska (1), Charmaine Childs (3), Gregory J. Czarnota (1,2)

(1) Sunnybrook Health Sciences Centre, Toronto, Canada , (2) University of Toronto, Toronto, Canada
(3) Sheffield Hallam University, Sheffield United Kingdom

Email: william.tran@sunnybrook.ca

ABSTRACT

Introduction: Functional imaging using diffuse optical spectroscopy (DOS) has been demonstrated capable of detecting response to neoadjuvant chemotherapy (NAC) in locally advanced breast cancer (LABC) within weeks after the start of treatment. Here we evaluate the efficacy of heterogeneity measures of DOS-based functional maps in predicting breast cancer response to treatment prior to the start of NAC.

Materials and Methods: LABC patients (n=37) planned for NAC had functional DOS maps and associated textural feature generated for parameters associated with tissue composition, and optical properties (deoxy-hemoglobin [Hb], oxy-hemoglobin [HbO2], total hemoglobin [HbT]), %Lipids, %Water, and scattering power [SP] prior to treatment. Textural features included *contrast (con)*, *correlation (cor)*, *energy(ene)*, and *homogeneity (hom)* and were normalized to fatty breast tissue. Patients were classified as responders or non-responders using clinical and pathological response criteria after treatment completion. DOS-Textural features were evaluated for predicting patient response from receiver-operating characteristic analysis, stepwise linear regression analysis and logistic regression modeling for combined parameters.

Results and Discussion: Data indicated that textural characteristics of pre-treatment DOS parametric maps can differentiate responding and non-responding patients with high sensitivity and specificity. Parameters Hb-ene and Hb–hom, resulted in the highest accuracy in predicting response to chemotherapy (%Sn/%Sp= 75.6-85.3% and an area under the curve (AUC) of 0.831. The results of this study demonstrate that tumour-contoured DOS-GLCM analysis can classify breast cancer response groups prior to starting NAC using baseline DOS measurements.

Keywords: Locally Advanced Breast Cancer, Optical Imaging, Diffuse Optical Spectroscopy, Imaging Biomarkers

Evaluating Histological Microfeatures and Microenvironment of Cancer *in Vivo* by Photoacoustic Techniques

Xueding Wang (1,2), Guan Xu (2), Janggun Jo (1), Cheri Deng (1), Chang Lee (3), Raoul Kopelman (3)

(1) Department of Biomedical Engineering, University of Michigan, Ann Arbor, MI 48109, USA
(2) Department of Radiology, University of Michigan, Ann Arbor, MI 48109, USA
(3) Department of Chemistry, University of Michigan, Ann Arbor, MI 48109, USA

Email: xdwang@umich.edu

ABSTRACT

Introduction: Majority of current studies on photoacoustic (PA) imaging are focused on the total signal magnitudes as the reflection of the macroscopic optical absorption by specific chemical contents at single or multiple optical wavelengths. Our recent research has demonstrated that the frequency domain power distribution of radio-frequency PA signals contains the microscopic information of the optically absorbing materials in the sample. In this research, I will introduce the recent development of quantitative PA methods for *in vivo* evaluation of histological microfeatures in biological tissues as well as potential clinical applications of these methods including the assessment of prostate cancer aggressiveness.

Materials and Methods: By performing PA scan over a broad spectrum covering the optical fingerprints of specific relevant chemical components, and then transforming the radio-frequency signals into the frequency domain, a 2D spectrogram, namely physio-chemical spectrogram (PCS) can be generated. The PCS presents the "optical signature" and the "ultrasonic signature" of tissue simultaneously in one 2D spectrogram, thus contains rich diagnostic information allowing quantification of not only contents but also histological microfeatures of various chemical components in tissue. Comprehensive analysis of PCS, namely photoacoustic physio-chemical analysis (PAPCA), could reveal the histopathology information in tissue and hold the potential to achieve comprehensive and accurate tissue characterization.

Results and Discussion: The experiment on human prostate tissues with Gleason grades confirmed by histopathology has validated the capability of PA spectral analysis in characterizing the Gleason patterns. Another experiment on non-alcoholic fatty liver disease (NAFLD) mouse models has demonstrated that, by quantifying the PCS at the optical absorption peaks of major chromophores in liver tissue including hemoglobin, lipid and collagen, PAPCA can non-invasively characterize the pathological changes correlated to steatosis and fibrosis in liver. Strategies of adapting this new technique to prostate cancer clinic will be discussed. In addition, I will also talk about the feasibility to evaluate cancer microenvironment by using PA imaging powered by nanoscale functional contrast agents. Some interesting results recently achieved on small-animal cancer models will be presented.

Keywords: Photoacoustic Imaging, Functional Imaging, Chemical Imaging, Tissue Characterization, Cancer Microenvironment, Nanoparticles, Contrast Agents

Multimodal Photoacoustic-Ultrasound Molecular Imaging and Biomarker Diagnostics

Roger Zemp (1), Robert Paproski (1,2), John Lewis (2)

(1) Department of Electrical and Computer Engineering, University of Alberta, Edmonton, Alberta, Canada, T6G 1H9
(2) Department of Experimental Oncology, University of Alberta, T6G 1Z2

Email: rzemp@ualberta.ca

ABSTRACT

Introduction: Improved toolsets for longitudinally monitoring prostate and other cancers to gage aggressiveness and to guide therapeutic interventions are urgently needed as frequency biopsies are not always possible or advisable. We present methods for multimodality photoacoustic-ultrasonic imaging and biomarker diagnostics with a focus on prostate cancer.

Materials and Methods: We have developed multi-modality porphysome nanodroplets capable of both ultrasound and photoacoustic imaging and demonstrated their passive accumulation in tumor models. These nanodroplets also act as cavitation nuclei for stimulating release of biomarkers into the bloodstream.

Results and Discussion: Uniquely, we have shown that ultrasound and nanodroplet treatments can stimulate release of large numbers of extracellular vesicles loaded with DNA, RNA, and protein biomarkers from the host tumor. We have identified a panel of 13 tumor-specific mutations, some of which are hallmarks of tumor aggressiveness. These could also be used to assess suitability of therapeutic targeting and to guide treatment planning.

Keywords: Ultrasound, Photoacoustic Imaging, Blood Biomarkers, Extracellular Vesicles.

Poster Abstracts

Differentiating Radionecrosis from Tumor Progression in Brain Metastases Treated with Radiosurgery: Utility of Intravoxel Incoherent Motion Perfusion MRI and Correlation with Histopathology

Jay Detsky (1), John Conklin (2), Julia Keith (3), Sean Symons (2), Arjun Sahgal (1), Chris Heyn (2), Hany Soliman (1)

(1) Department of Radiation Oncology, Sunnybrook Health Sciences Centre, Toronto, ON, Canada, M4N 3M5
(2) Department of Medical Imaging, Sunnybrook Health Sciences Centre, Toronto, ON Canada M4N 3M5
(3) Department of Pathology, Sunnybrook Health Sciences Centre, Toronto, ON Canada M4N 3M5

Email: jay.detsky@sunnybrook.ca

ABSTRACT

Introduction: Radiation necrosis occurs in 5-25% of patients who undergo stereotactic radiosurgery (SRS) for brain metastases. Standard imaging is poor at differentiating tumour progression from radiation necrosis. Intravoxel incoherent motion (IVIM) uses MRI diffusion-weighted imaging (DWI) to assess regional perfusion fraction without IV contrast. We investigated the utility of IVIM to differentiate recurrent tumor from radionecrosis after SRS.

Materials and Methods: Patients who had SRS for brain metastases and subsequently underwent surgical resection of what was thought to be either tumor progression or necrosis were included in this study. On the 3T MRI preceding surgery, regions of interest were contoured around enhancing lesions on the post-Gd T1-weighted images and transferred to DWI images (with multiple b-values from 0 to 1,000 s/mm^2) using automated co-registration. The perfusion fraction (f) was calculated using asymptotic fitting and the mean f (f_{mean}) and 90th percentile for f (f_{90}) as well as mean ADC (ADC_{mean}) and 10th percentile for ADC (ADC_{10}) were calculated. Pathology was evaluated as the percentage of viable tumor, tumor necrosis, or radiation necrosis.

Results and Discussion: Nine patients were included; one patient had two lesions removed in two surgeries four months apart, for a total of 10 lesions. The primary site of disease was lung (n=4), breast (n=3), rectal (n=1) and melanoma (n=1). One lesion exhibited pure necrosis while the other nine were mixed; five were predominantly (>70%) tumor, three predominantly necrosis, and one was equal parts of both. The perfusion fraction was significantly higher in cases with predominantly tumor compared to those with predominantly necrosis (f_{mean} = 10.2 ± 0.7 versus 8.3 ± 1.2, p = 0.02; f_{90} = 21.3 ± 2.1 versus 14.9 ± 2.5, p = 0.004). ADC did not differentiate tumor from necrosis (ADC_{mean} = 1.0 ± 0.2 versus 1.2 ± 0.4, p = 0.5; ADC_{10} = 0.6 ± 0.3 versus 0.8 ± 0.3, p = 0.35).

The IVIM perfusion fraction is useful in differentiating recurrent tumor from radionecrosis in patients with brain metastases treated with SRS. This is the first study to evaluate IVIM against the gold standard (histopathology) and needs to be validated in a larger cohort.

Keywords: Brain Metastases; Magnetic Resonance Imaging; Perfusion; Radiation Necrosis; Intravoxel Incoherent Motion

Optical Coherence Tomography Spectral Analysis for Detecting Apoptosis *In Vitro* and *In Vivo*

Golnaz Farhat (1,2), Anoja Giles (1,2), Michael C. Kolios (3), Gregory J. Czarnota (1,2)

(1) Imaging Research and Radiation Oncology, Sunnybrook Health Sciences Centre, Toronto, ON, Canada, M4N 3M5
(2) Departments of Radiation Oncology and Medical Biophysics, University of Toronto, Toronto, ON, Canada, M4N 3M5
(3) Ryerson University, Department of Physics, Toronto, Ontario, Canada, M5B 2K3

Email: golnaz.farhat@sunnybrook.ca

ABSTRACT

Introduction: Apoptosis, a form of programmed cell death, is characterized by a series of predictable morphological changes at the subcellular level including fragmentation of mitochondria and the nucleus, cell membrane blebbing and the eventual fragmentation of the cell into apoptotic bodies. These structural transformations affect the light scattering properties of cells. We present a spectroscopic optical coherence tomography (OCT) method for detecting changes in subcellular morphology related to apoptosis *in vitro* and *in vivo*.

Materials and Methods: Acute myeloid leukemia cells were treated with cisplatin to undergo apoptosis. *In vitro* OCT data were acquired from treated cell samples at multiple times over a 48-hour period. For the *in vivo* study, AML tumours were grown in the hind leg of SCID mice. The mice were treated with cisplatin and/or radiation and OCT data were acquired 24 hours later. Spectral parameters were extracted from the acquired OCT signals by calculating the integrated backscatter (IB) and the spectral slope (SS) of the OCT signal's backscatter spectrum.

Results and Discussion: The *in vitro* results indicated an increase in the IB and a decrease in the SS with treatment duration, with the most significant changes occurring 24 to 48 hours after the start of treatment. Striking morphological transformations in the cells and their nuclei were observed in histology slides prepared from cell samples in this same time period. Similar trends were observed *in vivo* with spectral parameters acquired from AML tumours. Our results provide a strong foundation from which future experiments may be designed to further understand the effect of cell morphology and the kinetics of apoptosis on the OCT signal and to demonstrate the feasibility of using this technique *in vivo*.

Keywords: Optical Coherence Tomography, Spectroscopy, Apoptosis, Treatment Monitoring.

Deep Learning in Clinical Cancer Therapy Response Monitoring

Mehrdad J. Gangeh (1,2), Peng Chen (1), William T. Tran (1,2), Gregory J. Czarnota (1,2)

(1) Imaging Research and Radiation Oncology, Sunnybrook Health Sciences Centre, Toronto, ON, Canada, M4N 3M5
(2) Departments of Radiation Oncology and Medical Biophysics, University of Toronto, Toronto, ON, Canada, M4N 3M5

Email: mehrdad.gangeh@sunnybrook.ca

ABSTRACT

Introduction: Therapeutic cancer response assessment in preclinical and clinical treatments is presently limited; results may not be available to the clinician for typically months. Quantitative ultrasound (QUS) methods provide a promising alternative framework that can non-invasively, inexpensively, and quickly assess early tumour response to cancer treatments using standard ultrasound equipment.

Materials and Methods: 102 patients with locally advanced breast cancer (LABC) who received neoadjuvant chemotherapy were imaged before and at 4 times during treatment, i.e., weeks 1, 4, 8 and pre-operatively. Spectral parametric maps were computed by employing QUS spectroscopy techniques. The patients were grouped into responders and non-responders based on their ultimate clinical and pathological response to treatment. A non-invasive computer-aided-theragnosis (CAT) system based on convolutional neural networks (CNNs) was developed for the early assessment of responses to neoadjuvant chemotherapy. "Mid-treatment" scans at three intervals during the course of treatment were compared with the baseline scans acquired before treatment onset ("pre-treatment"). Patches of 64 × 64 pixels were extracted from differentiated scans and submitted to the CNN for training and testing. The CNN comprised three main layers including *convolutional*, *pooling*, and *fully-connected* layers. The implementation of the network was accomplished using the Caffe library and the results of classification were compared with handcrafted texture parameters extracted from the parametric maps using local binary patterns (LBP).

Results and Discussion: The results of the classification using the developed CAT system based on deep learning indicated an improvement of performance up to 10% compared to a CAT system with handcrafted features using the LBPs. Accuracies of 90%, 82%, and 86% were achieved using the proposed CAT system after 1, 4, and 8 weeks of treatment, respectively. In this study, an advanced machine learning technique based on deep learning was proposed, for the first time, in the application of cancer response monitoring. The effectiveness of the developed method was assessed on 102 LABC patients treated with neoadjuvant chemotherapy. The proposed system achieves a promising accuracy early after the start of treatment. The results of this study would permit clinicians to receive feedback and switch to alternate treatments far earlier, in a step towards the goals of *personalized medicine*.

Keywords: Quantitative Ultrasound, Deep Learning, Machine Learning, Locally Advanced Breast Cancer

Cone-Beam CT Image Contrast and Attenuation-Map Linearity Improvement (CALI) for Brain Stereotactic Radiosurgery Procedures

Sayed Masoud Hashemi (1), Young Lee (1,4), Markus Eriksson (2), Håkan Nordström (2), James Mainprize (3), Arjun Sahgal (1), William Y. Song (1,4), Mark Ruschin (1,4)

(1) Dept. of Radiation Oncology, University of Toronto, Toronto, ON, Canada
(2) Elekta AB, Stockholm, Sweden
(3) Sunnybrook Research Institute, Toronto, ON, Canada
(4) Medical Physics Dept. Ryerson University, Toronto, ON, Canada

Email: masoud.hashemi@sunnybrook.ca

ABSTRACT

Introduction: The Leksell Gamma Knife Icon (Elekta AB, Stockholm, Sweden) integrates a Cone Beam CT (CBCT) image-guidance system that facilitates frameless planning and treatment delivery. The CBCT system provides the stereotactic reference, which together with co-registration of the planning image volume and the CBCT volume gives the transformation mapping of the planned isocenter positions to stereotactic coordinates. The Icon CBCT system employs a half-cone geometry to accommodate the existing treatment couch. This geometry increases the amount of artifacts and together with other physical imperfections causes image inhomogeneity and contrast reduction. The accuracy of the co-registration depends on the quality of the CBCT volume images. As a result, improving CBCT image is an essential step and is the focus of this study. A Contrast and Attenuation–map (CT#) Linearity Improvement (CALI) framework is proposed here to improve the homogeneity of the volume images, increase the soft tissue contrast, and to improve the accuracy of the CBCT CT#.

Materials and Methods: Our proposed framework includes a preprocessing step, involving a shading and beam-hardening artifact correction, and a post-processing step to correct the dome/capping artifact caused by the spatial variations in x-ray energy generated by bowtie-filter. Our shading correction algorithm relies solely on the acquired projection images (i.e. no prior information required) and utilizes filtered-back-projection (FBP) reconstructed images to generate a segmented bone and soft-tissue map. Ideal projections are estimated from the segmented images and a smoothed version of the difference between the ideal and measured projections is used in correction. The proposed beam-hardening and dome artifact corrections are segmentation free. This improves the robustness of the method by making it independent of segmentation errors.

Results and Discussion: The CALI was tested on CatPhan, as well as patient images acquired on the Icon system. The resulting clinical brain images show substantial improvements in soft contrast visibility, revealing structures such as ventricles and lesions which were otherwise un-detectable in FBP-reconstructed images. The linearity of the reconstructed attenuation-map was also improved, resulting in more accurate CT# (Table 1).

Keywords: CBCT Image Guidance, Artifact Correction, Soft Tissue Contrast Improvement.

True Value (HU)	Teflon	Derlin	Acrylic	Polystyrene	LDPE	PMP
	941:1060	**344:387**	**92:137**	**-65:-29**	**-121:-87**	**-220:-172**
Without Correction	871	365	176	19	-32	-69
With Correction	951	323	87	-58	-126	-187

Table 1: Comparison of the linearity of the CT numbers using the sensitometry slice of Catphan phantom, with and without the proposed corrections. True values are from CatPhan 503 manual.

Volumetric Ultrasound-Mediated Blood-Brain Barrier Opening Using a Large Aperture Phased Array Controlled via Passive Beamforming of Microbubble Emissions

Ryan M. Jones (1,2), Meaghan A. O'Reilly (1,2), Lulu Deng (1), Kogee Leung (1), Kullervo Hynynen (1,2,3)

(1) Physical Sciences Platform, Sunnybrook Research Institute, Toronto, Ontario, Canada, M4N 3M5
(2) Department of Medical Biophysics, University of Toronto, Toronto, Ontario, Canada, M5G 1L7
(3) Institute of Biomaterials and Biomedical Engineering, University of Toronto, Toronto, Ontario, Canada, M5S 3G9

Email: rmjones@sri.utoronto.ca

ABSTRACT

Introduction: Focused ultrasound (FUS) in combination with systemically injected microbubbles (MBs) can temporarily and selectively open the blood-brain barrier (BBB) [1], enabling targeted drug delivery to the brain. Previous studies have demonstrated that spectral characteristics of the MB emissions occurring during FUS BBB opening, measured using single-element passive detectors, are correlated with the biological effects of the exposures [2], which has led to the development of acoustic emissions-based feedback controllers [3]. The objective of the current study was to investigate if passive acoustic mapping (PAM), which uses an array of passive detectors to provide information regarding the spatial extent of MB activity [4], can be used to control FUS BBB opening over large cerebral volumes.

Materials and Methods: The array used in this study consisted of 256 transducer modules arranged in a sparse, simulation-optimized [5] configuration on a 30 cm diameter hemispherical shell. Each module contained 3 concentric cylindrical PZT4 elements driven in the lateral mode, with operating frequencies of 306, 612, and 1224 kHz. The transmit and receive frequencies for a given sonication were selected using in-house developed circuitry. Experiments were performed on Male New Zealand White rabbits (2.1-4.0 kg). The animals were coupled to the array via a water bath and any hair within the beam path was removed from their heads. A solution of Definity™ MBs was delivered via an ear vein catheter 10 s prior to each exposure. The array was electronically focused through the intact rabbit skull to a point within the brain without aberration correction. Ultrasound pulse trains (9 x 750 μs bursts, 250 μs spacing) were delivered at a 1 Hz PRF and 612 kHz driving frequency. The receiver signals were captured at the end of each burst using a multichannel receiver (250 μs capture, 10 MS/s sampling rate) at the subharmonic frequency, and PAM was performed [4]. The driving pressure was linearly increased following each pulse train (25 kPa step size) until spatially coherent subharmonic activity was observed at the target location, at which point the sonication was terminated. MRI was performed at 3T for targeting, to detect BBB opening, and to monitor for tissue damage.

Results and Discussion: Our data suggests that when coherent subharmonic activity is detected near the target location (0.47 ± 0.04 MPa estimated *in situ*), the threshold for BBB opening has been exceeded. Proximal target volumes were treated with constant pressure exposures (6 x 6 points/grid, 1 mm point spacing, 9 x 750 μs bursts/point, 0.7 Hz PRF/point, 2 min) at 50-75% of the value needed to generate this MB behavior, similar to our single-element control approach [3]. At the 50% target level no detectable tissue damage was seen on post-treatment MRI, however, at the 75% level hypointense regions were occasionally observed by T2*w imaging suggesting red blood cell extravasation or minor hemorrhage. Weekly repeat treatments up to 5 weeks in length (BBB opening volume per treatment of 230 ± 70 mm^3) were well tolerated. These results suggest that volumetric FUS BBB opening is feasible using a large aperture array, and that PAM is a promising tool for treatment control. The spatial information provided by PAM is expected to improve the sensitivity and specificity of acoustic emissions-based controllers.

Differentiation of Apoptosis/Necrosis from Active Tumour in Mice with Chemical Exchange Saturation Transfer (CEST) MRI

Wilfred W. Lam (1), Jonathan H. Klein (1,2,3), Farah Hussein (2), Christine Tarapacki (2), Gregory J. Czarnota (1,2,3,4), Greg J. Stanisz (1,3,5)

(1) Physical Sciences, Sunnybrook Research Institute, Toronto, ON, Canada
(2) Department of Radiation Oncology, Sunnybrook Health Sciences Centre, Toronto, ON, Canada
(3) Department of Medical Biophysics, University of Toronto, Toronto, ON, Canada
(4) Department of Radiation Oncology, University of Toronto, Toronto, ON, Canada
(5) Department of Neurosurgery and Pediatric Neurosurgery, Medical University of Lublin, Lublin, Poland

Email: lamw@sri.utoronto.ca

ABSTRACT

Introduction: Chemical Exchange Saturation Transfer (CEST) MRI is sensitive to the magnetization of hydrogen in dissolved proteins in exchange with that of water. Different chemical groups in these proteins can be probed by sweeping the frequency of applied radiofrequency energy, giving a CEST spectrum. This is potentially sensitive to the composition of tumours. We identified image intensity differences between apoptosis/necrosis and active tumour and compared them with histologically stained images.

Materials and Methods: Human breast cancer cells (MDA-MB-231) were injected into the hind limb of SCID mice (n = 6). The resulting tumours were imaged on a 7T animal MRI. CEST spectra were acquired for a single slice at the centre of the tumour. After imaging, the mice were treated with chemotherapy and imaged again following 24 h. The animals were sacrificed and tumours excised and assayed with TUNEL, which identifies apoptosis and necrosis. ROIs were manually drawn on the images around TUNEL-positive and negative regions. The mean CEST spectrum was calculated for each and compared using a paired t-test.

Results and Discussion: The CEST spectra of the apoptosis/necrosis ROI were different from those of active tumour for all mice (means shown in Fig. 1). The frequency offset of maximum separation, 1.83 ppm, was the same for the mean spectra of both baseline and treated mice. The magnetization transfer ratio (MTR) at this offset was significantly different between apoptosis/necrosis and active tumour for both baseline and treated mice (Fig. 2). Figure 3 shows good agreement between the post chemo MTR map at this offset and histology.

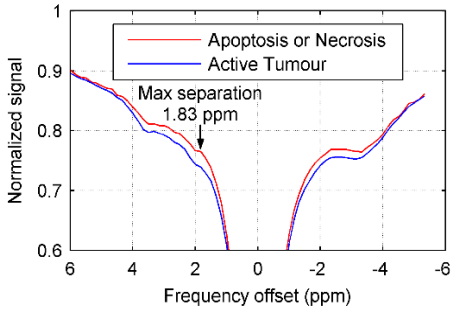

Figure 3. Mean CEST spectra of baseline mice for apoptosis/necrosis and active tumour ROIs. Spectra for treated mice were similar.

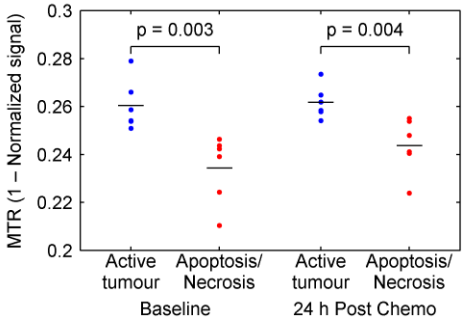

Figure 1. Magnetization transfer ratio (MTR) for all mice at the frequency offset of maximum separation. The bars indicate the means.

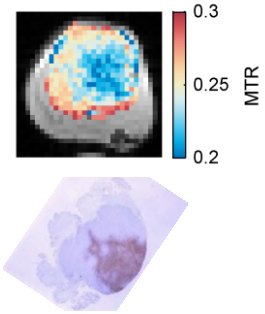

Figure 2. Post chemo MTR map at 1.83 ppm and TUNEL slide from the same mouse.

Keywords: Cancer, Response Monitoring, Pre-Clinical Imaging, MRI, CEST

Compound Speckle Model Reduces Contrast Ultrasound Variability in a Patient-Derived Xenograft Model of Renal Cell Carcinoma

Matthew R. Lowerison (1,7), Ann F. Chambers (1,3), Hon S. Leong (3,5,6), Nicholas E. Power (2,3), James C. Lacefield (1,4,7)

Departments of (1) Medical Biophysics, (2) Oncology, (3) Surgery, (4) Electrical and Computer Engineering, (5) Pathology and Laboratory Medicine, (6) Microbiology and Immunology, Western University, London, ON, Canada, N6A 5C1
(7) Robarts Research Institute, Western University, London, ON, Canada, N6A 5B7

Email: mloweri@uwo.ca

ABSTRACT

Introduction: Renal cell carcinoma (RCC) accounts for the majority of diagnosed kidney cancers in Canadian adults and is the most lethal of all genitourinary cancers. Targeted therapies, such as sunitinib, are initially effective in most cases as RCC is highly dependent on tumor-driven angiogenesis. However, an estimated 25-30% of patients exhibit *de novo* resistance to their prescribed front-line therapy. There is currently no established means to identify resistant patients before tumor progression is observed months after the beginning of therapy. This presentation outlines the development of high-frequency ultrasound imaging methods to evaluate treatment strategies for patients with metastatic RCC in a high-throughput patient-derived xenograft (PDX) assay in the chicken embryo chorioallantoic membrane (CAM). We demonstrate that analysis of the first-order speckle statistics of nonlinear contrast-enhanced ultrasound (CEUS) images reduces the variability in tumor perfusion quantification, particularly for estimates of blood volume, and reduces the sensitive/resistant classification ambiguity caused by heterogeneous tumor samples.

Materials and Methods: Tumor engraftment procedures were performed on the ninth day of embryonic development (EDD-9) with at least 300 embryos per patient tumor. At the time of nephrectomy, 5-9 tumor core biopsies (8 mm diameter) were extracted to obtain adequate coverage of the entire tumor and any nearby metastases. Biopsies were sectioned into ~2 mm^3 fragments and implanted into the CAM immediately after scoring of the chorionic epithelium. Tumors were treated every two days with either 3 µL (10 µM) of sunitinib or DMSO as a control until imaging on EDD-18.
B-mode, power Doppler, and CEUS images were acquired using a Vevo 2100 ultrasound system (VisualSonics Inc.). All image analysis was performed using MATLAB (The MathWorks Inc., Natick, MA). Contrast signal intensity was modeled as a compound distribution of exponential probability density functions with a gamma weighting function. The gamma probability weighting function served as an approximation for log-normally distributed flow velocities in tumor vasculature. Tumor fragments were classified as sunitinib sensitive or resistant based on significant reductions in tumor vascularity and blood volume as measured by power Doppler and CEUS, respectively.

Results and Discussion: Implantation of tumor specimens into the CAM resulted in high engraftment efficiencies (take rate of 60-80%) relative to those observed in immunocompromised mice. We observed intratumoral functional heterogeneity both within untreated core biopsies and in the response to antiangiogenic therapy. First-order speckle analysis reduced the coefficient of variation of CEUS estimates of blood volume compared to conventional CEUS methods (CoV of 0.554 vs. 0.828, Brown–Forsythe test p-value < 0.05) and thereby improved patient classification confidence. Preliminary results indicate that tumor pathology and drug-resistant phenotype are conserved when patient biopsies are grown on the CAM. This PDX model, in conjunction with high-frequency ultrasound, permits functional tumor heterogeneity studies to be completed within two weeks, making this an approach that could guide the selection of drugs, anticipate resistances, and predict patient outcomes in a clinically relevant time window.

Keywords: Contrast-Enhanced Ultrasound, Speckle, Renal Cell Carcinoma, Patient-Derived Xenograft

Comparing the Diagnostic Accuracy of Luminal Water Imaging with Diffusion-Weighted and Dynamic Contrast-Enhanced MRI for Evaluation of Prostate Cancer.

Shirin Sabouri (MSc)(1), Silvia D. Chang (MD)(2,3,4), Richard Savdie (MD)(2), Edward C. Jones (MD)(5), S. Larry Goldenberg (MD)(2,3), Peter C. Black (MD)(2,3), Piotr Kozlowski (PhD)(2,3,4,6)

(1) Department of Physics and Astronomy, University of British Columbia, Vancouver, BC, Canada
(2) Department of Urologic Sciences, University of British Columbia, Vancouver, BC, Canada
(3) Vancouver Prostate Centre, Vancouver, BC, Canada
(4) Department of Radiology, University of British Columbia, Vancouver, BC, Canada
(5) Department of Pathology and Laboratory Medicine, University of British Columbia, Vancouver, BC, Canada
(6) UBC MRI Research Center, Vancouver, BC, Canada

Email: sabouri@phas.ubc.ca

ABSTRACT

Purpose: To compare the diagnostic accuracy of luminal water imaging (LWI) with diffusion-weighted imaging (DWI) and dynamic contrast-enhanced (DCE) MRI, and evaluate the significance of including LWI in a multi-parametric MRI (MP-MRI) protocol for diagnosis of prostatic carcinoma (PCa).

Introduction: LWI is a new application of quantitative T_2 mapping that has shown promising results for detection, localization, and grading of PCa [1]. This technique measures the fractional amount of luminal water which has been shown to be proportional to the percentage area of luminal space in prostatic tissue [2]. In this study we compare diagnostic accuracy of LWI, DCE, and DW-MRI, and various combinations of these techniques in detecting and grading PCa.

Material and Methods: 18 patients with biopsy proven PCa were examined with LWI, DWI, and DCE MRI at 3T prior to undergoing radical prostatectomy. From LWI data, signal decay curve for each voxel was extracted and fitted to multi-exponential function to generate maps of parameters called: $T_{2\text{-short}}$, $T_{2\text{-long}}$, $_{gm}T_2$, LWF, A_{short}, A_{long}, and N as described in [1]. From the set of four DWI images, with b values: 0, 100, 500, and 1000 s/mm^2, apparent diffusion coefficient (ADC) was calculated by using the Stejskal-Tanner equation. For processing DCE MRI data, concentration of contrast agent in the tissue was calculated from PD and T1W images as described in [3]. By fitting the concentration of contrast agent in tissue to the extended Kety model [4] values of pharmacokinetic parameters: K^{trans}, ν_e, and ν_p were calculated. Maps of all MR parameters were correlated to whole-mount histology through registration. Receiver operating characteristics (ROC) analysis was used to evaluate the diagnostic accuracy of individual and combined MR parameters in detection of PCa. Correlations with Gleason score (GS) were evaluated using Spearman's rank correlation test.

Results and Discussions: Among the single MRI techniques, the highest area under ROC curve (AUC) value in all regions of investigation (AUC: 0.78 in the entire prostate, 0.96 in peripheral zone (PZ), 0.92 in glandular transition zone (TZ)) . Among the combined MRI techniques, the highest AUC values (0.82 in the entire prostate, 0.97 in PZ, and 0.98 in glandular TZ) were obtained from combination of LWI with either DCE or DW-MRI. The strongest correlation with GS was achieved by LWI both in PZ (ρ:-0.76, $P<0.001$) and in glandular TZ (ρ:-0.64, $P<0.001$). Results of this pilot study show that LWI performs equally well or better than DCE and DWI in detection of PCa and in correlation with GS in PZ and glandular TZ. This technique can potentially be included in clinical MP-MRI protocols to increase the accuracy of diagnosis of PCa. To engage LWI in clinical settings, a study with higher number of patients and broader range of GS is required.

Keywords: Prostate Cancer, Quantitative T_2 Mapping, Multi-Parametric MRI, DWI, DCE MRI.

Response Monitoring of Breast Cancer Patients Receiving Neo-Adjuvant Chemotherapy using QUS, Texture and Molecular Features

Lakshmanan Sannachi (1,2), William Tran (1,2), Mehrdad Gangeh (1,2), Sonal Gandhi (3), Frances Wright (4), Gregory J. Czarnota (1,2)

(1) Imaging Research and Radiation Oncology, Sunnybrook Health Sciences Centre, Toronto, ON, Canada, M4N 3M5
(2) Departments of Radiation Oncology and Medical Biophysics, University of Toronto, ON, Canada, M4N 3M5
(3) Division of Medical Oncology, Sunnybrook Health Sciences Centre, Toronto, ON, Canada, M4N 3M5
(4) Division of General Surgery, Sunnybrook Health Sciences Centre, Toronto, ON, Canada, M4N 3M5

Email: Lakshmanan.Sannachi@Sunnybrook.ca

ABSTRACT

Introduction: The aim of this study was to classify clinical/pathological response to neoadjuvant chemotherapy using quantitative ultrasound and receptors status in patients with locally advanced breast cancer.

Materials and Methods: Ninety six patients were enrolled into the study. Breast tumors were scanned with a 10 MHz clinical ultrasound system prior to chemotherapy treatment, during the first, fourth and eighth week of treatment, and prior to surgery. QUS spectral parameters, backscatter parameters, and scatterer spacing were calculated from ultrasound radio frequency (RF) data within the tumor region of interest. Additionally, texture features were extracted from all QUS parametric maps. Prior to therapy, all patients underwent a core needle biopsy and histological subtypes and most common receptors such as ER, PR and Her2 status were recorded. Patients were classified into three treatment response groups based on pathological analysis: complete pathological response (CR), partial response (PR) and non-responders (NR). These classifications were determined by examining tumor diminishment and levels of cellularity of the mastectomy specimens after treatment. Response classifications from QUS parameters, receptors status and pathological were compared. The classification analyses were performed on extracted parameters using supper vector machine classifier (SVM) to differentiate CR, PR, and NR at all scan time points.

Results and Discussion: QUS parameters classified three response groups with accuracies of 53%, 60% and 58% at week 1, 4, and 8, respectively. Similarly, combination of three receptors status predicted three response groups with accuracies of 38%, 37% and 50% at week 1, 4, and 8, respectively. The best prediction of treatment response was achieved with the combination QUS parameters and receptors status with accuracies of 78%, 86% and 83% at week 1, 4, and 8, respectively. The recurrence free survival of complete and partial responding patients determined based on clinical/pathology and combined QUS parameters and molecular features were higher than non-responding patients ($p < 0.001$). However, both parameters did not reveal significant difference between CR and PR at all scan time points. This work demonstrated the potential of quantitative ultrasound and status of most common type of receptors for predicting the three types of response of breast tumours to chemotherapy early and guiding the treatment planning of refractory patients.

Keywords: Breast cancer, Neo-adjuvant Chemotherapy, Tumor Response, Quantitative Ultrasound, Texture Analysis

Finite Element Simulation of the Propagation of Ultrasound Waves in a Bubbly Medium and Theoretical Considerations for Treatment Optimization

AJ Sojahrood (1), H. Haghi (1), R Krshafian (1), MC Kolios (1)

(1) Ryerson University, Department of Physics, Toronto, Ontario, Canada, M5B 2K3

ABSTRACT

Introduction: After administration of the microbubbles (MBs) to the medium, the attenuation increases and the sound speed of the medium changes. The alteration in attenuation and sound speed are nonlinear and depend on the MB size and frequency and pressure of the ultrasound pulse. The increased attenuation shields the propagation of waves to the focal region and can decrease the effectiveness of the application (e.g. drug delivery) or result in unwanted heating outside of the focal region (e.g. HIFU enhanced heating). Detailed information on the attenuation and sound speed in the medium is needed to optimize the applications.

Materials and Methods: In this work the nonlinear dynamics of the MBs is classified in terms of the linear resonance frequency (fl) of the MBs for ($0.2fr<fr<4fr$) and for acoustic pressures of $1kPa<P<4$ MPa. By using our original nonlinear model, the pressure dependent attenuation and sound speed of the bubbly medium are calculated and classified. The propagation of the focused waves in the bubbly medium is simulated using finite element method (FEM) and applying the pressure dependent attenuation and sound speed.

Results and Discussion: FEM simulations show that the increase in the attenuation due to the presence of the MBs, may entirely shield the target and even eliminate the focal region. This effect is very significant when the sonication frequency is chosen close to the linear resonance frequency of the MBs. However, the frequency of the sonication and the pressure amplitude at the surface of the transducer can be optimized. In this regard, by using the pressure-dependent resonance frequency of the MBs the attenuation of the pre-focal target can be minimized while the attenuation at the focus is maximum. This will result in a minimum loss in the focal pressure and enhances the drug delivery applications of MBs and improves the quality of contrast-enhanced ultrasound response monitoring.

Keywords: Treatment Planning, Drug Delivery, Microbubbles, Nonlinear Oscillations, Attenuation, Finite Element Method

Predicting Clinical and Pathological Response of Breast Tumours to Neoadjuvant Chemotherapy Using Pre-Treatment Textural Features of Diffuse Optical Spectroscopic Images

William Tyler Tran (1,2,3), Ali Sadeghi-Naini (1,2), Lee Chin (1), Lakshmanan Sannachi (1,2), Elyse Watkins (1), Sharon Lemon Wong (1), Belinda Curpen (1,2), Maureen Trudeau (1,2), Sonal Gandhi (1,2), Martin Yaffe (1), Elzbieta Slodkowska (1), Charmaine Childs (3), Gregory J. Czarnota (1,2)

(1) Sunnybrook Health Sciences Centre, Toronto, Canada
(2) University of Toronto, Toronto, Canada
(3) Sheffield Hallam University, Sheffield United Kingdom

Email: william.tran@sunnybrook.ca

ABSTRACT

Introduction: Functional imaging using diffuse optical spectroscopy (DOS) has been demonstrated capable of detecting response to neoadjuvant chemotherapy (NAC) in locally advanced breast cancer (LABC) within weeks after the start of treatment. Here we evaluate the efficacy of heterogeneity measures of DOS-based functional maps in predicting breast cancer response to treatment prior to the start of NAC.

Materials and Methods: LABC patients (n=37) planned for NAC had functional DOS maps and associated textural feature generated for parameters associated with tissue composition, and optical properties (deoxy-hemoglobin [Hb], oxy-hemoglobin [HbO2], total hemoglobin [HbT]), %Lipids, %Water, and scattering power [SP] prior to treatment. Textural features included *contrast (con), correlation (cor), energy(ene),* and *homogeneity (hom)* and were normalized to fatty breast tissue. Patients were classified as responders or non-responders using clinical and pathological response criteria after treatment completion. DOS-Textural features were evaluated for predicting patient response from receiver-operating characteristic analysis, stepwise linear regression analysis and logistic regression modeling for combined parameters.

Results and Discussion: Data indicated that textural characteristics of pre-treatment DOS parametric maps can differentiate responding and non-responding patients with high sensitivity and specificity. Parameters Hb-ene and Hb–hom, resulted in the highest accuracy in predicting response to chemotherapy (%Sn/%Sp= 75.6-85.3% and an area under the curve (AUC) of 0.831. The results of this study demonstrate that tumour-contoured DOS-GLCM analysis can classify breast cancer response groups prior to starting NAC using baseline DOS measurements.

Keywords: Locally Advanced Breast Cancer, Optical Imaging, Diffuse Optical Spectroscopy, Imaging Biomarkers

Biodegradable Theragnostic Agents for Breast Cancer Detection and Therapy using Photoacoustic Technique

Yanjie Wang (1,2,3), Michael C. Kolios (1,2,3)

(1) Physics Department, Ryerson University, Toronto, Ontario, Canada
(2) Institute for Biomedical Engineering, Science and Technology (iBEST), a partnership between Ryerson University and St. Michael's Hospital, Toronto, Ontario, Canada
(3) Keenan Research Centre for Biomedical Science of St. Michael's Hospital, Toronto, Ontario, Canada

Email: mkolios@ryerson.ca

ABSTRACT

Introduction: Breast cancer is one of the most common malignancies, causing serious impacts on women's physical and mental health.Conventional chemotherapy often results in severe side effects due to the non-targeted drug delivery. In this study, we developed optical-triggered imaging anddrug delivery nanoparticles (NPs) for breast cancer diagnosis and treatment using photoacoustic (PA) technique. This NP consists of a core made of gold nanoparticles (GNPs) dissolved in perfluorocarbon liquid, surrounded by a polymer PLGA shell. The GNPs serve as PA contrast agents and as fuels for laser-induced particle vaporization. The chemo drug Paclitaxel can be loaded in the PLGA shell. The particle surface was bounded by Herceptin to achieve active targeting. Herceptin is an FDA approved antibody that targets the human epidermal growth factor receptor-2 (HER-2), highly expressed in breast cancer tissues of certain individuals. These NPs would provide a multimodal tool allowing for improved breast cancer imaging, while providing increased efficiency of drug release due to targeting, and a potential reduction of side effects in patient.

Materials and Methods: The PLGA particles loaded with GNPs/Paclitaxel/fluorescent dyeswere synthesized by the double emulsion technique. For the covalent attachment of Herceptin onto the PLGA particle surface, 1-ethyl-3-(3-dimethylaminopropyl)-carbodiimide (EDC) reagent were used to conjugate the primary amine group of Herceptin with the free carboxylic end group of PLGA, forming a connecting amide bond. The targeted and non-targeted PLGA particles loaded with GNPs/Paclitaxel were incubated with breast cancer cells for certain time intervals. The cells loaded with PLGA-GNPs were irradiated with a pulsed laser. The PLGANP cell uptake and cell viability were tested using flow cytometry and MTT assay.

Results and Discussion: The effects of laser-induced particle vaporization on cell viability and PLGA particle drug loading and delivery capacities were demonstrated in cell culture experiments. Our results showed that after incubation PLGA-GNPs with MCF7 cells for 6 and 12 hours, the laser induced vaporization reduced the cell viability to 19% and 20%, respectively. For cells exposed to PLGA-PAC particles for 6 and 12 hours, the survival rates decreased to 30% and 28%, respectively. This result indicated that the chemo drug was delivered into the cells by the PLGA parties. Laser induced vaporization inside cells demonstrated strong therapeutic efficiency. The cancer cell active targeting and PLGA particles uptake by the SKBRS cells was test using flow cytometry. The results showed that cell uptake increased about 30% compared with cell uptake without targeting. The combination of utilizing laser activation, active targeting and drug release couldachieve a localized therapeutic dose using a minimally invasive nature of treatment.

Keywords: Nanomaterials, Drug Delivery, Photoacoustic, Theranostic, Cancer Therapy

Ultrasound and Photoacoustic Analysis of HT-29 and AML Cell Pellets at 200 MHz

Lauren A. Wirtzfeld, Eric M. Strohm, Michael C. Kolios

Department of Physics, Ryerson University, Toronto, Ontario, Canada
Institute for Biomedical Engineering, Science and Technology (iBEST), a partnership between Ryerson University and St. Michael's Hospital, Toronto, Canada
Keenan Research Centre for Biomedical Science of St. Michael's Hospital, Toronto, Canada

Email: lauren.wirtzfeld@ryerson.ca

ABSTRACT

Introduction: Scattering of ultrasound from biological tissues is a complex process not fully understood. Continued study of ultrasound scattering and photoacoustic signal generation is essential to fully understand the imaging modalities and allow for the most information to be extracted in diagnostic imaging applications. The relationship between tissue structure and scattering varies based on scattering sources and number density which change with imaging frequency. Collections of cells in three-dimensional arrangements have not been well characterized at frequencies above 100 MHz, the resolution volume is on the order of a cell, for either ultrasound or photoacoustic imaging. This study presents ultrasound and photoacoustic data from an in vitro model of packed cell at 200 MHz, where the resolution volume is on the order of the size of the cell nucleus.

Materials and Methods: Pellets approximately 150 μm thicker of HT-29 (human colon carcinoma) and OCI-AML5 (human acute myeloid leukemia) cells were created by centrifuging cells in a 9 mm wide glass bottom well. For each cell line, one pellet was made with the nucleus dyed using DRAQ5 and one pellet was made with the cytoplasm dyed using Neutral Red. A photoacoustic microscope that was designed and built by Kibero GmbH (Saarbrucken, Germany), was used to image the cell pellets. A 200 MHz f#1 transducer and a 532 nm laser were used. The focus of both the ultrasound and laser were kept at the centre of the pellets for all measurements. Photoacoustic signals were therefore obtained from either the cytoplasm or nucleus, depending on the dye used.

Results and Discussion: Reconstructed B-mode images show good signal to noise ratio for both photoacoustic and ultrasound imaging. Both sets of images show speckle patterns suggesting that echoes from multiple sources or scatterers are being received, although the resolution volume is small, comparable to the size of a cell. Several minima are observed in the power spectra over the transducer bandwidth, which will continue to be analyzed in future work examining the acoustic backscatter and photoacoustic signal spectra. Detailed analysis of these spectra, including simulations, will help us relate the photoacoustic and ultrasound signals. This will enable us to better understand the data received from aggregates of cells when the resolution is on the order of a single cell.

Keywords: Photoacoustics; High-Frequency Ultrasound; HT-29; AML; Cell Pellets

Potential Benefit of Rotational Radiation Delivery

Jason Vickress (1), Michael Lock (1,2), Aaron Leung (1), Stewart Gaede (1,2), Rob Barnett (1,2), Slav Yartsev (1,2)

(1) Departments of Oncology and Medical Biophysics, Western University, London, ON, Canada N6A 5C1
(2) London Regional Cancer Program, London Health Sciences Centre, London, ON, Canada, N6A 4L6

Email: slav.yartsev@lhsc.on.ca

ABSTRACT

Introduction: It is a standard procedure to collect detailed electronic records of a patient's specific treatment plan during radiation therapy. These records include diagnostic images, radiation plan details, delivery parameters, and dose distributions. With the incorporation of patient specific parameters, predictive models can be helpful to guide a physician's decision. Our objective is to develop and verify a predictive model for survival and time to recurrence of liver cancer patients using retrospectively collected clinical patient data.

Materials and Methods: Selected patient information was collected from 195 liver cancer patients treated at the London Regional Cancer Program. Outcome information included survival, disease recurrence, and blood work (tumour markers). All radiation therapy planning parameters were included in the analysis including Biologically Effective Dose (BED). Predictive models were created using Cox regression for both survival and recurrence data. Patients were split into two almost equal groups: rotational delivery (RD) and fixed beam delivery (FB) for modeling and verification, respectively. All variables selected for the Cox regression analysis. For Kaplan-Meir curves, patients were split across the median hazard ratio.

Results and Discussion: Predictive model has been developed for liver cancer patients treated with radiation therapy. Even with almost twice the average GTV size, the RD group showed comparable survival and time to recurrence as the FB group. For patients with a Child Pugh score of A, increased radiation dose showed a significant survival benefit. Our data suggest that sufficient dose to the healthy tissue around the tumour improves disease free survival if rotational delivery of radiation is used Only parameter describing normal tissue irradiation V24 had a significant effect on disease free survival (DFS) for the rotational delivery group with a hazard ratio (HR) of 0.495, whereas patients treated with fixed beams delivery were significantly affected by increased radiation dose to the tumour. For all patients poor liver function parameters and tumour size reduced overall survival. VMAT and Tomotherapy performed the same as 3DCRT and IMRT, despite treating higher risk patients (with larger GTVs). Including dosimetric parameters not previously analyzed can provide additional insight in important patient outcomes in radiation therapy

Keywords: Radiation Therapy; Predictive Models; Liver Cancer; Rotational Delivery.

Contacts

Innovations in Cancer Therapy & Treatment Monitoring
November 16-17, 2016

No.	Title	Last	First	Institution	Email
1	Ms.	Bamberger	Lucy	Elekta	lucy.bamberger@elekta.com
2	Dr.	Bauman	Glenn	London Health Sciences Centre	glenn.bauman@lhsc.on.ca
3	Ms.	Berndl	Elizabeth	Ryerson University	eberndl@ryerson.ca
4	Dr.	Bok	Tae-Hoon	Ryerson University	tbok@ryerson.ca
5	Dr.	Chin	Lee	Sunnybrook Health Sciences Centre	lee.chin@sunnybrook.ca
6	Dr.	Chow	Edward	Sunnybrook Health Sciences Centre	Edward.Chow@sunnybrook.ca
7	Dr.	Chu	William	Sunnybrook Health Sciences Centre	william.chu@sunnybrook.ca
8	Dr.	Chugh	Brige	Sunnybrook Health Sciences Centre	brige.chugh@sunnybrook.ca
9	Dr.	Cloutier	Guy	University of Montreal	guy.cloutier@umontreal.ca
10	Dr.	Czarnota	Gregory	Sunnybrook Health Sciences Centre	gregory.czarnota@gmail.com
11	Dr.	Demore	Christine	Sunnybrook Research Institute	cdemore@ieee.org
12	Dr.	Deng	Cheri	University of Michigan	cxdeng@umich.edu
13	Dr.	Desmond	Kimberly	Sunnybrook Research Institute	kdesmond@sri.utoronto.ca
14	Dr.	Detsky	Jay	Sunnybrook Health Sciences Centre	jay.detsky@sunnybrook.ca
15	Mr.	Fadhel	Muhanned	Ryerson University	mfadhel@ryerson.ca
16	Dr.	Farhat	Golnaz	Sunnybrook Health Sciences Centre	golnaz.farhat@gmail.com
17	Dr.	Feleppa	Ernest	Riverside Research	efeleppa@RiversideResearch.org
18	Dr.	Foster	Stuart	Sunnybrook Research Institute	stuart@sri.utoronto.ca
19	Dr.	Gangeh	Mehrdad	Sunnybrook Health Sciences Centre	mehrdad.gangeh@utoronto.ca
20	Dr.	Ghai	Sangeet	Exact Imaging	Sangeet.Ghai@uhn.ca
21	Ms.	Giles	Anoja	Sunnybrook Health Sciences Centre	anoja.giles@sunnybrook.ca
22	Dr.	Goertz	David	Sunnybrook Research Institute	goertz@sri.utoronto.ca
23	Dr.	Greenleaf	James	Mayo Clinic School of Medicine	jfg@mayo.edu
24	Dr.	Guha	Chandan	Montefiore Medical Center	CGUHA@montefiore.org
25	Dr.	Hall	Tim	University of Wisconsin	tjhall@wisc.edu
26	Dr.	Harris	Emma	Institute of Cancer Research	eharris@icr.ac.uk
27	Dr.	Hashemi	Masoud	Sunnybrook Health Sciences Centre	masoud.hashemi@sunnybrook.ca
28	Dr.	Heyn	Chris	Sunnybrook Health Sciences Centre	chris.heyn@utoronto.ca
29	Ms.	Hoey	Christianne	Sunnybrook Research Institute	christianne.hoey@mail.utoronto.ca
30	Dr.	Holland	Christy	University of Cincinnati	hollanck@ucmail.uc.edu
31	Mr.	Hupple	Clinton	iThera Medical	clinton.hupple@ithera-medical.com
32	Mr.	Hysi	Eno	Ryerson University	eno.hysi@ryerson.ca
33	Dr.	Iqbal	Fawaad	Durham Regional Cancer Centre	fiqbal@lakeridgehealth.on.ca
34	Mr.	Jafari Sojahrood	Amin	Ryerson University	amin.jafarisojahrood@ryerson.ca
35	Mr.	Jones	Ryan	Sunnybrook Research Institute	rmjones@sri.utoronto.ca
36	Dr.	Karshafian	Raffi	Ryerson University	karshafian@ryerson.ca
37	Dr.	Keller	Brian	Sunnybrook Health Sciences Centre	Brian.Keller@Sunnybrook.ca
38	Dr.	Kerbel	Robert	Sunnybrook Research Institute	robert.kerbel@sri.utoronto.ca
39	Dr.	Khodabandehlou	Khosrow	Sunnybrook Health Sciences Centre	khosrow.khodabandehlou@sunnybrook.ca

40	Dr.	Klein	Jonathan	Sunnybrook Health Sciences Centre	jonathan.klein@sunnybrook.ca
41	Dr.	Kolios	Michael	Ryerson University	mkolios@ryerson.ca
42	Dr.	Kozlowski	Piotr	University of British Columbia	piotr.kozlowski@ubc.ca
43	Dr.	Kripfgans	Oliver	University of Michigan	greentom@umich.edu
44	Dr.	Kumaradas	Carl	Ryerson University	ckumarad@ryerson.ca
45	Dr.	Lacefield	James	Western University	jlacefie@uwo.ca
46	Dr.	Lam	Wilfred	Sunnybrook Research Institute	lamw@sri.utoronto.ca
47	Dr.	Lau	Angus	Sunnybrook Research Institute	angus.lau@sri.utoronto.ca
48	Mrs.	Law	Niki	Sunnybrook Health Sciences Centre	niki.law@sunnybrook.ca
49	Mr.	Lee	Julian	Alpinion	julian.lee@alpinionusa.com
50	Mr.	Lee	Jae Seoup	Sunnybrook Health Sciences Centre	polobear88@gmail.com
51	Dr.	Liu	Stanley	Sunnybrook Health Sciences Centre	stanley.liu@sunnybrook.ca
52	Mr.	Lowerison	Matthew	Robarts Research Institute	mloweri@uwo.ca
53	Dr.	Mayr	Nina	University of Washington	ninamayr@uw.edu
54	Mr.	McCartney	Trevor	Elekta	trevor.mccartney@elekta.com
55	Mr.	Mestman	Scott	Philips	scott.mestman@philips.com
56	Dr.	Muleki-Seya	Pauline	University of Illinois Urbana-Champaign	muleki@illinois.edu
57	Mr.	Nicolae	Alexandru	Sunnybrook Health Sciences Centre	Alexandru.Nicolae@sunnybrook.ca
58	Dr.	Oakden	Wendy	Sunnybrook Research Institute	wendy.oakden@gmail.com
59	Dr.	O'Brien	William	University of Illinois	wdo@uiuc.edu
60	Dr.	Oelze	Michael	University of Illinois Urbana-Champaign	oelze@illinois.edu
61	Dr.	O'Reilly	Meaghan	Sunnybrook Research Institute	moreilly@sri.utoronto.ca
62	Ms.	Pan	Lihong	GE Healthcare	lihong.pan@ge.com
63	Dr.	Pang	Georgi	Sunnybrook Health Sciences Centre	georgi.pang@sunnybrook.ca
64	Dr.	Paszat	Lawrence	Sunnybrook Health Sciences Centre	lawrence.paszat@ices.on.ca
65	Dr.	Popescu	Tony	BC Cancer Agency	tpopescu@bccancer.bc.ca
66	Dr.	Porter	Tyrone	Boston University	tmp@bu.edu
67	Ms.	Quiaoit	Karina	Sunnybrook Health Sciences Centre	karina.quiaoit@sunnybrook.ca
68	Dr.	Ravi	Anath	Sunnybrook Health Sciences Centre	ananth.ravi@gmail.com
69	Ms.	Ray	Jessica	Sunnybrook Research Institute	jessica.ray@mail.utoronto.ca
70	Dr.	Razani	Marjan	Ryerson University	mrazani@ryerson.ca
71	Dr.	Rohrbach	Daniel	Riverside Research	drohrbach@riversideresearch.org
72	Mrs.	Sabouri	Shirin	University of British Columbia	sabouri@phas.ubc.ca
73	Dr.	Sadeghi-Naini	Ali	Sunnybrook Research Institute	ali.sadeghi@sri.utoronto.ca
74	Dr.	Sahgal	Arjun	Sunnybrook Health Sciences Centre	arjun.sahgal@sunnybrook.ca
75	Dr.	Sannachi	Lakshmanan	Sunnybrook Health Sciences Centre	laksmanan@gmail.com
76	Dr.	Seker	Fazila	MaRS Innovation	fseker@marsinnovation.com
77	Dr.	Skorski	Lech W.	Sunnybrook Research Institute	lskorski@sri.utoronto.ca
78	Dr.	Soliman	Hany	Sunnybrook Health Sciences Centre	hany.soliman@sunnybrook.ca
79	Dr.	Song	William	Sunnybrook Health Sciences Centre	william.song@sunnybrook.ca
80	Dr.	Spayne	Jacqueline	Sunnybrook Health Sciences Centre	jacqueline.spayne@sunnybrook.ca
81	Dr.	Stanisz	Greg	Sunnybrook Research Institute	greg.stanisz@gmail.com
82	Dr.	Strohm	Eric	University of Toronto	eric.strohm@utoronto.ca

83	Ms.	Sutton	Kayla	University of Toronto	kayla.sutton@mail.utoronto.ca
84	Ms.	Tchistiakova	Ekaterina	Sunnybrook Health Sciences Centre	ekaterina.tchistiakova@sunnybrook.ca
85	Dr.	Tome	Wolfgang	Montefiore Medical Center	wolfgang.tome@einstein.yu.edu
86	Mr.	Tran	William	Sunnybrook Health Sciences Centre	william.tran@sunnybrook.ca
87	Dr.	Vesprini	Danny	Sunnybrook Health Sciences Centre	danny.vesprini@sunnybrook.ca
88	Ms.	Wang	Yan	Ryerson University	yanjie.wang@ryerson.ca
89	Dr.	Wang	Xueding	University of Michigan	xdwang@umich.edu
90	Dr.	Wirtzfeld	Lauren	Ryerson University	lauren.wirtzfeld@ryerson.ca
91	Dr.	Xu	Helen	Sunnybrook Health Sciences Centre	helen.xu@sunnybrook.ca
92	Dr.	Yartsev	Viatcheslav	London Regional Cancer Program	slav.yartsev@lhsc.on.ca
93	Dr.	Yuh	William	University of Washington	assistmedicalimaging@seattlecca.org
94	Dr.	Zemp	Roger	University of Alberta	rzemp@ualberta.ca